Science of the Total Environment 977 (2025) 179369

Contents lists available at ScienceDirect

Science of the Total Environment

journal homepage: www.elsevier.com/locate/scitotenv

Assessing Pan-Canada wildfire susceptibility by integrating satellite data with novel hybrid deep learning and black widow optimizer algorithms

Khabat Khosravi [a,b], Ashkan Mosallanejad [c], Sayed M. Bateni [d,e], Dongkyun Kim [f], Changhyun Jun [g,*], Ali Reza Shahvaran [h], Aitazaz A. Farooque [b,i,j,**], Massoud Karbasi [a], Mumtaz Ali [k]

[a] Department of Natural Resources, College of Agriculture and Natural Resources, Razi University, Kermanshah, Iran
[b] School of Climate Change and Adaptation, University of Prince Edward Island, Charlottetown, PE, Canada
[c] Department of Civil and Environmental Engineering, Iran University of Science and Technology, Tehran, Iran
[d] Department of Civil, Environmental and Construction Engineering and Water Resources Research Center, University of Hawaii at Manoa, Honolulu, HI, USA
[e] UNESCO-UNISA Africa Chair in Nanoscience and Nanotechnology College of Graduates Studies, University of South Africa, Muckleneuk Ridge, Pretoria 392, South Africa
[f] Department of Civil and Environmental Engineering, Hongik University, Seoul, South Korea
[g] School of Civil, Environmental and Architectural Engineering, College of Engineering, Korea University, Seoul, Republic of Korea
[h] Ecohydrology Research Group, Department of Earth and Environmental Sciences, University of Waterloo, Waterloo, Canada
[i] Canadian Center for Climate Change and Adaptation, University of Prince Edward Island, St Peters Bay, PE, Canada
[j] Faculty of Sustainable Design Engineering, University of Prince Edward Island, Charlottetown, PE, Canada
[k] UniSQ College, University of Southern Queensland, Springfield Campus, QLD 4301, Australia

HIGHLIGHTS

- Wildfire susceptibility mapping was conducted on a nationwide in Canada.
- Novel hybrid of LSTM-GWO, RNN-GWO, BiLSTM-GWO, and BiRNN-GWO were implemented.
- The results revealed that the hybrid BiLSTM-BWO model outperformed other models.
- Approximately 62.3 %, 13.4 %, and 24.3 % of Canada classified as having low, moderate, and high susceptibility.
- Saskatchewan, Manitoba, British Columbia and Alberta identified as very high wildfire susceptible provinces.

GRAPHICAL ABSTRACT

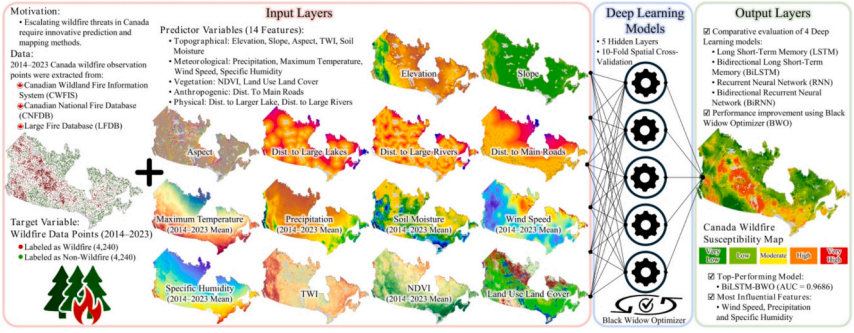

ARTICLE INFO

Editor: Jay Gan

Keywords:
Wildfire
Susceptibility mapping

ABSTRACT

In light of the rising frequency of severe wildfires and their widespread socio-ecological impacts, it is essential to develop cost-effective and reliable methods for accurately predicting and mapping wildfire occurrences. This study aimed to develop several novel deep-learning models to determine the probability of wildfire occurrence on a national scale in Canada by integrating remote sensing data, deep learning, and metaheuristic algorithms. In the present study, novel standalone long short-term memory (LSTM), recurrent neural network (RNN),

* Corresponding author.
** Correspondence to: Aitazaz A. Farooque, Canadian Centre for Climate Change and Adaptation, University of Prince Edward Island, St Peters Bay, PE, Canada.
E-mail addresses: cjun@cau.ac.kr (C. Jun), afarooque@upei.ca (A.A. Farooque).

https://doi.org/10.1016/j.scitotenv.2025.179369
Received 6 October 2024; Received in revised form 4 April 2025; Accepted 5 April 2025
Available online 15 April 2025
0048-9697/© 2025 The Authors. Published by Elsevier B.V. This is an open access article under the CC BY-NC-ND license (http://creativecommons.org/licenses/by-nc-nd/4.0/).

Bidirectional long short-term memory
Black widow optimizer
Canada

bidirectional LSTM (BiLSTM), and bidirectional RNN (BiRNN) models were developed, and these were hybridized with a black widow optimizer (BWO). To train and test the models, 4240 historical (2014–2023) large wildfire locations were collected across Canada. Fourteen wildfire-related predictors were used to map wildfire susceptibility, with the Gini coefficient determining each predictor's importance in wildfire occurrence. Finally, the developed models were evaluated and tested using the area under the receiver operating characteristic curve (AUC), and other statistical error metrics. During the testing stage, the hybrid BiLSTM-BWO model outperformed the other models (AUC = 0.9686), followed by RNN-BWO (AUC = 0.9683), LSTM-BWO (AUC = 0.9672), BiRNN-BWO (AUC = 0.9643), BiLSTM (AUC = 0.9420), LSTM (AUC = 0.9367), BiRNN (AUC = 0.9247) and RNN (AUC = 0.8737). Based on the BiLSTM-BWO model, 19.7 %, 42.6 %, 13.4 %, 14.5 %, and 9.8 % of Canada was classified as having very low, low, moderate, high, and very high susceptibility to future wildfires, respectively. Saskatchewan, Manitoba, British Columbia and Alberta were among the provinces with large areas of very high susceptibility to wildfires, while Prince Edward Island and Newfoundland and Labrador from Atlantic Canada had the lowest probability of wildfire occurrence. According to the Gini coefficient, windspeed, land use and land cover, precipitation, specific humidity and maximum temperature had the strongest impact on wildfire susceptibility across Canada. This study highlights the effectiveness of the developed hybrid models in wildfire prediction and their potential to improve land management, wildfire prevention, and mitigation strategies in Canada's future.

1. Introduction

Wildfires have been reported to affect approximately 4 % of the global land area annually (Doerr and Santín, 2016; Tang et al., 2021). These natural disasters are a major environmental concern because they have the potential to severely damage broad areas of forest, leading to habitat destruction, severe loss of biodiversity, and increased soil erosion. The resulting changes to the landscape due to wildfires can also disrupt hydrological cycles, increase flood risk, and reduce ecosystems resilience. Wildfires are also a major source of air pollution, releasing substantial amounts of carbon dioxide (CO_2) and other greenhouse gases, particulate matter (PM2.5), and other harmful pollutants, potentially impacting climate change.

Canada has been more severely affected by a record-breaking series of wildfires in recent years (i.e., 2023). According to data from Canada's National Forestry Database, more than 8000 wildfires occur annually, burning an average of over 2.1 million hectares of land. Hanes et al. (2019) stated that lightning was responsible for starting 59 % of the wildfires, and these lightning-induced fires contributed to 93 % of the total burned area. Particularly, according to the Canadian Interagency Forest Fire Centre, wildfires burned over 13 million hectares in Canada in the first seven months of 2023, with an estimated 1 billion tons of CO_2 emitted into the atmosphere (Wang et al., 2024). This represents a significant public health concern, as a Canadian study estimated that wildfire-related PM2.5 exposure increases the relative risk of all-cause, cardiovascular, and respiratory mortality by 1.019, 1.017, and 1.019, respectively (Chen et al., 2021). Moreover, a Global Fire Assimilation System (GFAS) report notes that the Canadian wildfire season typically runs from May through September, and in 2023, total PM2.5 emissions were 6.6 times higher than the average over the past 20 years (Di Giuseppe et al., 2018). Canadian wildfires also influence the global air quality, particularly in the Northern Hemisphere (Chen et al., 2025a, b).

Wildland fire activity is a complex process that depends on several geoenvironmental factors such as ignition source, fuel composition, weather, and topography. Recently, a variety of methods, including empirical/statistical, semi-empirical, physics-based, and artificial intelligence (AI) models have been developed to enhance the accuracy of wildfire occurrence predictions based on these factors. However, given the complexity of wildfire dynamics, simple linear methods generally fail to produce reliable results. Empirical methods, which rely on statistical correlations between wildfire occurrences and their causal factors, are highly sensitive to the quality and quantity of data available and often struggle to capture the nonlinear relationships involved (Abatzoglou and Brown, 2012; Xue et al., 2012), while semi-empirical models which are a computational or mathematical model that combines theoretical principles with empirical data complicated the modeling approach and based on energy conservation principles typically do not distinguish between different heat transfer mechanisms (Mell et al., 2007). In contrast, physics-based approaches simulate fire occurrence by incorporating hydrodynamics, combustion processes, and energy transfer dynamics (Mell et al., 2007).

However, these methods depend on several assumptions, such as soil moisture, vegetation characteristics, and land cover, which can reduce their predictive accuracy (Massada et al., 2011; Sturtevant et al., 2009). As a result, AI models have become increasingly important in wildfire modeling, including fire detection, fire weather, occurrence, susceptibility, behavior, effects, and fire management (Jain et al., 2020).

Recently, machine learning and deep learning models have been integrated with geographic information systems (GIS) and remote sensing data to more accurately predict wildfire-prone areas. Arrue et al. (2000) designed an intelligent system for forest fire detection using artificial neural networks (ANNs) and infrared image processing to identify true wildfires, while Liu et al. (2015a) investigated forest fire detection using ANNs and multiple attributes (e.g., flame, heat, light, and radiation). Support vector machine (SVM) has also been implemented to automatically detect wildfires from video frames (Zhao et al., 2011) and a genetic algorithm (GA) has been used for multi-objective optimization of light detection and ranging (LiDAR)-based fire detection (Cordoba et al., 2004). Another study was conducted for early fire detection based on hierarchical Bayesian networks (BNs) (Ko et al., 2010), while an adaptive neural fuzzy inference system (ANFIS) was used to detect forest fire-prone regions using spatial data (Angayarkkani and Radhakrishnan, 2011). Numerous studies have employed AI-based models for wildfire prediction (Prasad and Ramakrishna, 2008; Wang et al., 2011; Li et al., 2015; Sayad et al., 2019; Horn et al., 2025; Masoudian et al., 2025). For example, Tran et al. (2023) used a group method of data handling (GMDH) algorithm combined with three metaheuristic models—teacher-learning-based optimization (TLBO), imperialist competitive algorithm (ICA), and biogeography-based optimization (BBO)—for wildfire modeling on Oahu Island, US. Their results revealed that GMDH-TLBO was the most accurate model, while standalone GMDH produced the weakest performance. Hong et al. (2018) utilized the Random Forest (RF) and Support Vector Machine (SVM) models for forest fire susceptibility mapping in Dayu County, China. The results indicated that the RF model demonstrated higher performance compared to the SVM model. Hong et al. (2019) integrated the Weights-of-Evidence (WOE) bivariate model with the Analytical Hierarchy Process (AHP) model for forest fire prediction in Huichang County, China, achieving an AUC between 0.91 and 0.94.

It is important to note that machine learning methods tend to be susceptible to environmental changes. In contrast, deep learning adapts to these changes via constant feedback. Deep-learning models can effectively analyze novel data sets due to their hidden layer architecture. Zhang et al. (2016) employed a deep convolutional neural network

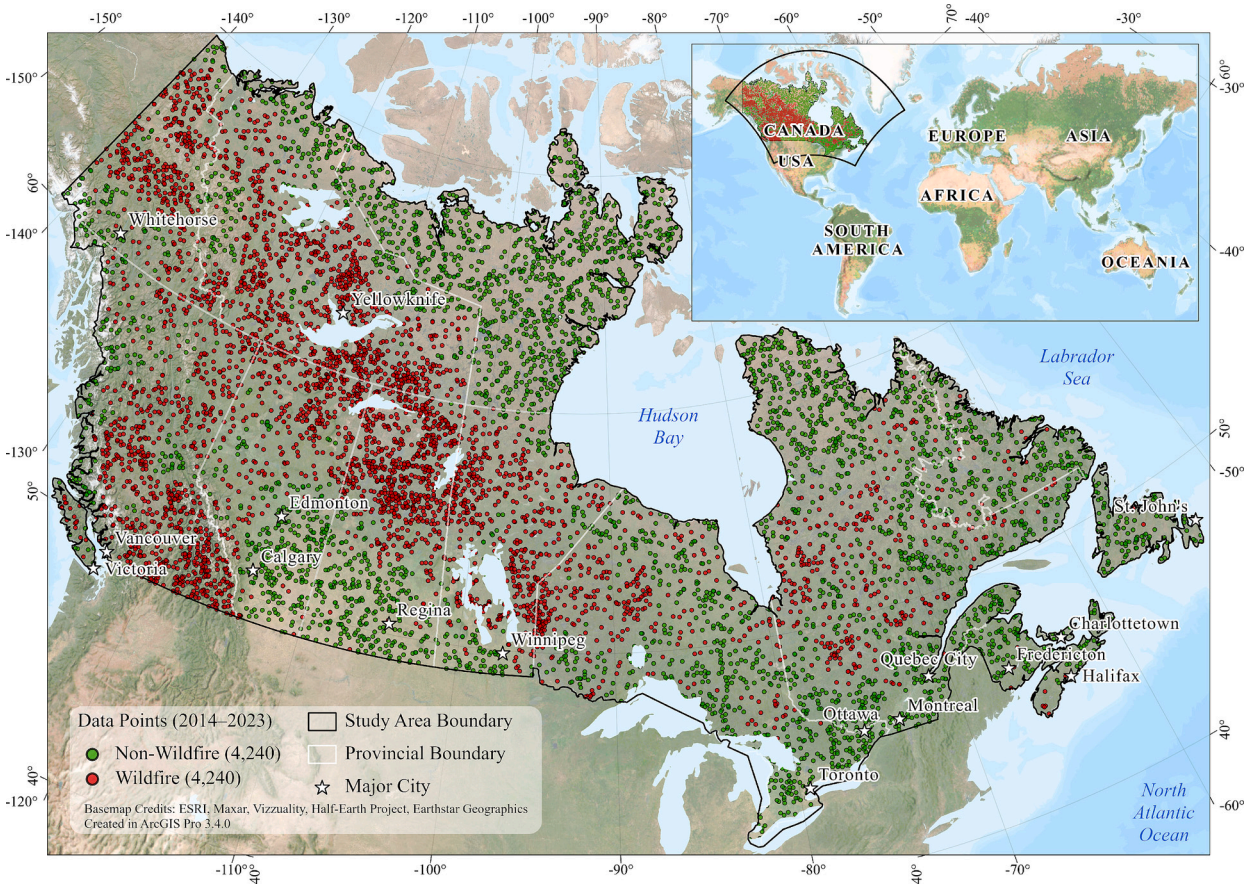

Fig. 1. Study area and collected historical (2014–2023) large wildfire locations.

(CNN) for forest fire detection using terrestrial-based images, while a follow-up study implemented early wildfire smoke detection based on an improved codebook model and a CNN (Zhang et al., 2018). A novel image-based fire detection approach has been proposed based on the combination of a deep learning network with multi-dimensional texture analysis based on higher-order linear dynamical systems (Barmpoutis et al., 2019). Rezaie et al. (2023) compared the prediction accuracy of GMDH and a CNN for wildfire modeling on the island of Maui, US, finding that the latter outperformed the former. Roy and Shome (2023) also optimized recurrent neural network (RNN)–long short-term memory (LSTM) architecture using an NSGA-II algorithm for IoT-driven fire detection systems. Their proposed model improved the accuracy to 95.05 % and reduced the false positive rate. Khennou and Akhloufi (2023) used a U-Net algorithm to improve wildland fire areas. They also used an FU-NetCastV2 deep-learning model designed for fire spread prediction and burned area mapping, achieving an accuracy of 94.6 % and outperforming previously reported models by 3.7 %. Masrur et al. (2023) implemented convolutional LSTM (ConvLSTM) for spatiotemporal wildfire modeling. Their proposed model was evaluated using a high-resolution wildfire spread dataset generated using a semi-empirical percolation model and satellite-observed wildfire spread data from California for the 2012–2021 period. Their findings demonstrated that attention-based models effectively predict fire front movements, aligning closely with established wildfire spread and biophysical dynamics. Janizadeh et al. (2023) implemented Partial Least Squares (PLS), boosting, bagging, and Bayesian algorithms combined with the Generalized Linear Model (GLM) to detect wildfire-prone areas in the Chalus Rood watershed, Iran. The results revealed that all developed models have a high accuracy in order of: PLS-GLM, boosted-GLM, bagging-GLM, and Bayesian-GLM models. Saha et al. (2023) applied Random Forest (RF), Multivariate Adaptive Regression Splines (MARS), and Deep Learning Neural Network (DLNN) models for forest fire susceptibility mapping in the Ayodhya Hill region, part of the Eastern Ghats Mountain Range in India. Their findings indicated that the DLNN algorithm achieved the highest prediction accuracy. Janizadeh et al. (2024) integrated the Light Gradient-Boosting Machine (LightGBM) model with three metaheuristic algorithms—Golden Jackal Optimization (GJO), Pelican Optimization Algorithm (POA), and Zebra Optimization Algorithm (ZOA)—for wildfire susceptibility mapping on Kaua'i, and Moloka'i islands, Hawaii, USA. They reported that the LightGBM-ZOA model achieved the highest accuracy (AUC = 0.9314), followed by LightGBM-GJO (AUC = 0.9308), LightGBM-POA (AUC = 0.9303), and the standalone LightGBM (AUC = 0.9228).

Though many other studies have employed deep-learning models for wildfire predictions (Li et al., 2018; Muhammad et al., 2018; Yuan et al., 2018; Jakubowski et al., 2019; Li et al., 2019; Wang et al., 2019), many of these studies are mostly based on terrestrial images for fire and smoke detection. Ramayanti et al. (2024) implemented the bivariate frequency ratio (FR) model and deep learning models, including CNN and LSTM, for mapping wildfire-prone areas on Maui Island, USA. The results demonstrated that the CNN model outperformed the other models. Moreover, these studies mostly implemented CNN models and did not utilize other types of deep learning, restricting the scope of more advanced models. In response to this, the present study proposes a wildfire susceptibility prediction approach that integrates satellite-derived data, deep learning, and a black widow optimizer (BWO). The present study utilizes geoenvironmental factors as model inputs, including topographic, meteorological, vegetation, and anthropogenic variables, to predict wildfire susceptibility. Canada has been severely affected by a series of wildfires annually. One of the basic approaches to managing and mitigating the effects of wildfires is preparing wildfire susceptibility maps. The main aims of the present study were to improve

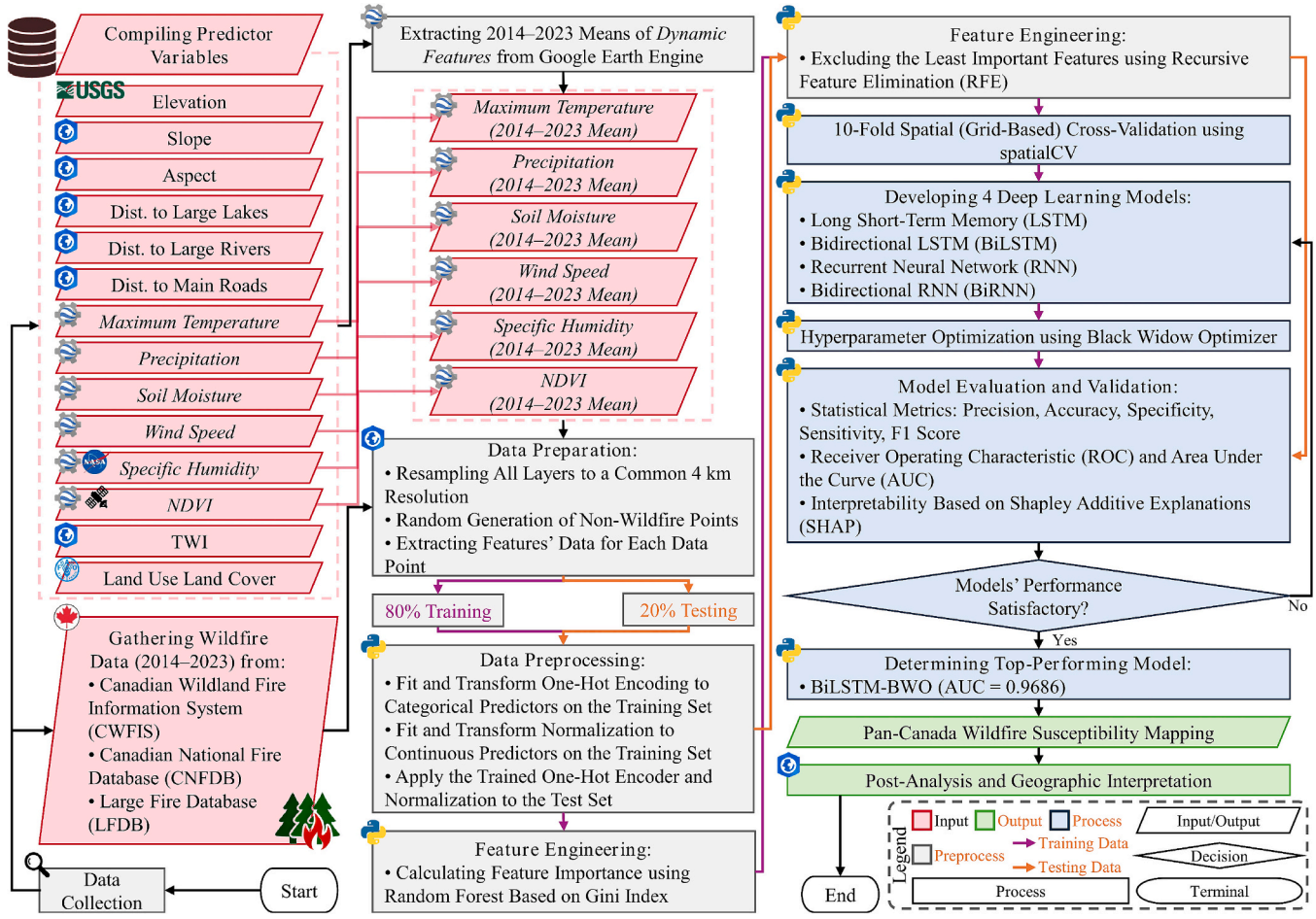

Fig. 2. Methodological flowchart employed in the present study.

wildfire susceptibility prediction and mapping for Canada for the first time, which is a wildfire hotspot country, and take advantage of feature/input importance selection using a random forest classifier and recursive feature elimination (RFE) for determine the optimal input scenario and identify the most influential input geoenvironmental variables on wildfire occurrence. To achieve these aims, LSTM, bidirectional LSTM (BiLSTM), RNN, and bidirectional RNN (BiRNN) models were built, and they hybridized with BWO to examine how much their prediction accuracy will be improved using the BWO metaheuristic algorithm. The proposed modeling framework was applied to Canada's national-scale wildfire susceptibility prediction successfully. To the best of our knowledge, this is the first attempt to implement BiLSTM and BiRNN models in natural hazard modeling.

2. Study area

Canada is the world's second-largest country by total area (9,984,670 km^2), although it ranks fourth by land area due to its abundant freshwater lakes. Spanning from the Atlantic Ocean in the east to the Pacific in the west, with the Arctic Ocean to the north, it has the world's longest coastline (243,042 km) and shares the longest land border with the United States (8891 km). Canada also shares a border with Greenland to the northeast (Fig. 1).

Canada can be divided into seven physiographic regions: Canadian Shield, Great Lakes–St. Lawrence Lowlands, Interior Plains, Appalachian region, Hudson Bay Lowlands, Western Cordillera, and the Arctic Archipelago. Boreal forests dominate much of the country, while ice is prevalent in the northern Arctic and the Rocky Mountains areas. The flat Canadian Prairies in the southwest are important areas of agriculture, while the Great Lakes feed into the St. Lawrence River in the southeast, a region that drives much of Canada's economy. With over 2,000,000 lakes—563 of which are larger than 100 km^2—Canada holds a significant portion of the world's freshwater, and it also has freshwater glaciers in the Rockies, Coast Mountains, and Arctic Cordillera. The average winter and summer temperatures vary widely across Canada. Summer highs on the east and west coasts typically reach 20–24 °C, while interior regions can reach 25–30 °C, occasionally exceeding 40 °C (Regina International Airport, 2015) which increases its susceptibility to wildfire.

3. Method

The conceptual modeling framework employed in this study involved several key steps: data collection, pre-processing, model development, model deployment (wildfire map generation), and performance evaluation (Fig. 2). Each step is explained in detail in the subsequent sections.

3.1. Data collection and inventory map

Compiling a wildfire inventory map is the most important step in developing machine learning models to identify wildfire-susceptible areas. This map is constructed using point-based historical wildfire locations and is used to assess the spatial relationship between wildfire occurrences and wildfire-related geoenvironmental factors. In this study, a comprehensive wildfire inventory map was collected, incorporating 4240 large wildfire occurrences (i.e. fires greater than 200 ha in final size) recorded over the past decade (2014–2023). The data were sourced from the National Burned Area Composite, Fire History Data,

Fig. 3. Photographs of recent wildfire events in Canada, showing their impact on the ecosystem, landscape and local communities (www.theatlantic.com, www.cbc.ca).

and Canadian Wildland Fire Information System (CWFIS) Datamart. Canada is experiencing a rising frequency and intensity of large wildfires. Starting in March 2023, Canada experienced an unprecedented series of wildfires that intensified by June/July, affecting all 13 provinces and territories, with major fires in British Columbia, Alberta, Nova Scotia, the Northwest Territories, Ontario, and Quebec (Fig. 3). The 2023 wildfire season became the most destructive in Canada's recorded history, burning an area of 184,961 km^2 by October 6—over six times higher than the long-term average and affecting approximately 5 % of the country's forested area (The State of Canada's Forests Report, 2023). The fires resulted in the deaths of eight firefighters and displaced between 185,000 to 232,000 people, with international aid helping to mitigate the disaster's impact (Smellie, 2023).

3.2. Generating non-wildfire data

The algorithm randomly samples candidate points within the study area using Python's built-in random module and computes each point's Euclidean distance to the nearest historical wildfire locations (red data points in Fig. 1). A candidate is accepted only if its distance exceeds a predefined threshold, set at 4 % of the average of the minimum and maximum distances among fire points, ensuring adequate spatial separation. This process repeats until 4240 non-wildfire points are collected (green data points in Fig. 1) or a maximum of 500,000 attempts is reached. To create a balanced model and reliable results, the number of wildfire and non-wildfire cases are recommended to be equal.

3.3. Spatial autocorrelation between wildfire and non-wildfire data

A spatial autocorrelation analysis was conducted using the Global Moran's I toolbox in ArcGIS Pro (v3.4.0), yielding a highly significant Moran's I value of 0.855, with a z-score of 160.59 and a *p*-value of 0.000. These results indicate a strong clustering pattern, confirming that the randomly generated non-wildfire points, positioned based on their distance from actual wildfire occurrences, are distinctly separated from wildfire clusters. This clear spatial distinction is beneficial, as it reduces ambiguity in machine learning-based wildfire susceptibility models by ensuring that each dataset maintains well-defined, non-overlapping spatial patterns.

3.4. Training and testing sets

In the present study, we employed binary classification for wildfire modeling, which involved inputting both wildfire and non-wildfire location data (Tehrany et al., 2014). Therefore, 4240 non-wildfire locations were also generated across the entire study as mentioned above. The wildfire and non-wildfire locations were assigned values of 1 and 0, respectively. Hold-out cross-validation with an 80:20 ratio was subsequently utilized to partition both wildfire and non-wildfire datasets. Specifically, 80 % of the historical wildfire locations were allocated for model training, while the remaining 20 % were reserved for testing purposes (Abdollahi and Pradhan, 2023).

In the next step, data from both 80 % of the wildfire and non-wildfire locations were combined to create the training dataset for the design, development, and hyperparameter tuning of the proposed model. The other 20 % of the wildfire and non-wildfire location data were combined

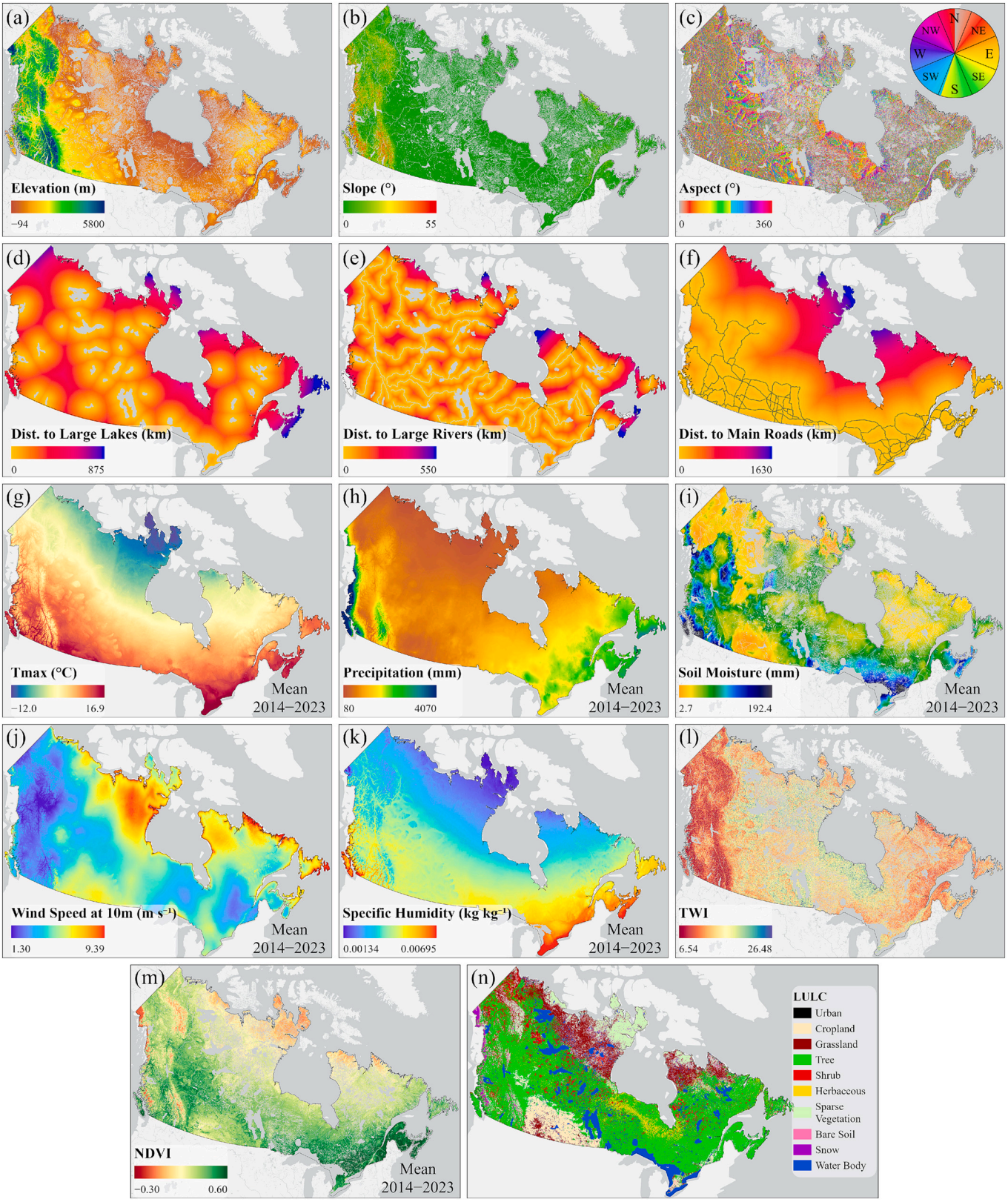

Fig. 4. Geoenvironmental wildfire-influencing factors used as inputs for the proposed model.

to create the testing dataset for model evaluation. The training dataset was overlaid with all 14 remaining wildfire-related factors, and their attributes (i.e. wildfire locations within each class of each parameter) were extracted using ArcGIS Pro (v3.4.0). These extracted attributes were prepared in Excel format and subsequently imported into Python 3.10 for model development.

3.5. *Wildfire-related geoenvironmental factors*

Wildfire-related geoenvironmental factors were selected for the

Table 1
Potential input geoenvironmental factors description.

Category	Geoenvironmental factor	Source	Spatial resolution	Importance
Topographic	Elevation	Digital elevation model-USGS	30 m	Wildfires are affected by elevation (Alizadeh et al., 2023) due to its association with rainfall, soil moisture, temperature, and vegetation cover
	Slope			Slope is associated with the soil moisture content, which affects wildfires (Iban and Sekertekin, 2022).
	Aspect			The aspect is associated with solar radiation, temperature, wind speed, soil moisture, and the distribution of plant species (Le et al., 2021).
	TWI			Areas with a higher TWI have a higher soil moisture content
	Soil moisture	TerraClimate (Abatzoglou et al., 2018)	~4 km	Regions with higher soil moisture levels are less prone to fire ignition (Achu et al., 2021).
Meteorological	Precipitation	ClimateNA (Mahony et al., 2022; Wang et al., 2016)	~4 km	Precipitation has a direct impact on wildfire through its impact on vegetation cover and soil moisture content
	Wind speed	TerraClimate (Abatzoglou et al., 2018)	~4 km	Higher wind speeds accelerate wildfire spread by carrying embers and providing more oxygen
	Specific humidity	NASA (McNally, 2018)	~11 km	Lower humidity leads to drier fuels and increases wildfire risk
	Mean maximum temperature	TerraClimate (Abatzoglou et al., 2018)	~4 km	Higher temperatures have a direct impact on wildfires, especially due to climate change and a longer drought season
Vegetation	LULC	FAO (Latham et al., 2014)	800 m	Some LULC types such as shrubland and conifer forests are more vulnerable to wildfires compared to wetlands and agricultural areas (Carmo et al., 2011; Moreira et al., 2001 and Moreira et al., 2009).
	NDVI	Government of Canada	1 km	The NDVI measures the greenness and the density of the vegetation
Anthropogenic	Distance from major roads	Government of Canada	4 km	Regions close to roads are more likely to experience anthropogenic impacts such as camping
Physical	Distance from major rivers	Government of Canada	4 km	Regions close to rivers have a higher soil moisture content
	Distance from lakes	Government of Canada	4 km	Regions close to lakes have a higher soil moisture content

[a]All geospatial layers are resampled to a uniform 4 km by 4 km Pan-Canadian grid using ArcGIS Pro (v 3.4.0). Resampling methods: Majority for slope, aspect, and LULC; Cubic Convolution for all other layers.

present study based on a literature review, data availability, and the characteristics of the study area, and then grouped into five key categories: meteorological, topographic, anthropogenic, vegetation, and physical (Fig. 4). The meteorological factors were mean annual total precipitation, wind speed, specific humidity and maximum temperature from 2014 to 2023. The topographic factors considered were elevation, slope, aspect, the topographic wetness index (TWI), and mean annual soil moisture (2014–2023), while the anthropogenic factor was the distance from main roads. The vegetation and physical factors were the distance from large lakes, distance from large rivers, land use and land cover (LULC) and the mean annual normalized difference vegetation index (NDVI) from 2014 to 2023. Finally, all datasets were converted to raster format and resampled to a uniform 4 km spatial resolution. The importance of each factor and the source database are summarized in Table 1. More information can be found in Jaafari et al. (2019), Rezaie et al. (2023), and Tran et al. (2023).

3.6. Data scaling

In machine learning, one-hot encoding is a widely utilized technique for managing categorical data, particularly when numerical input is required by most algorithms. Categorical variables, such as land use and land cover (LULC), must be transformed into a suitable numerical format during the data pre-processing stage. To ensure the data remains non-ordinal, one-hot encoding was applied to mitigate the risk of machine learning models erroneously assigning greater importance to higher numerical values. The implementation of one-hot encoding allowed the categorical variables to be represented in a binary format, preserving the non-ordinal nature of the data and enhancing model accuracy. Continues data were normalized using the Min-Max Normalization equation:

$$X_{norm} = (X - X_{min})/(X_{max} - X_{min}) \quad (1)$$

where, X_{norm} is the normalized value, X is the original value, X_{min} is the minimum value in the dataset, and X_{max} is the maximum value in the dataset.

All data processing and modeling tasks were conducted in Python 3.10, leveraging its extensive libraries for data manipulation and machine learning.

3.7. Input variable selection

3.7.1. Feature importance using a random forest classifier

Although there is no standard set of predictive factors for wildfire susceptibility and the importance of these factors differs between study areas, it is essential to analyze the relationship between geo-environmental factors and the probability of wildfire occurrence and exclude those factors with low/null effectiveness to improve the results (Panahi et al., 2023). To achieve this, the random forest model can be used to extract feature importance (Pal, 2005). Determining feature importance can reduce the dimensionality of the data, reducing the complexity of the resulting model and thus ensuring that it is more transparent, easier to interpret, and faster to run. Each decision tree in a random forest model splits its nodes based on specific feature values to reduce the level of impurity, similar to Gini impurity in classification problems. Features that consistently lead to a significant reduction in impurity across the ensemble of trees are considered more important. The significance of each feature is determined by averaging the reduction in impurity it causes across all the trees in the forest. After the model is trained, feature importance can be assessed by randomly shuffling the values of each feature and observing the corresponding drop in accuracy. Features that lead to a significant decline in accuracy when altered are deemed more critical to the model.

The Gini Index (GI) is calculated by taking 1 minus the sum of the squared probabilities for all classes. It can be mathematically represented as (Breiman et al., 1984):

$$GI = 1 - \sum_{i=1}^{n} (p_i)^2 \quad (2)$$

where P_i represents the probability of an element being classified for a distinct class.

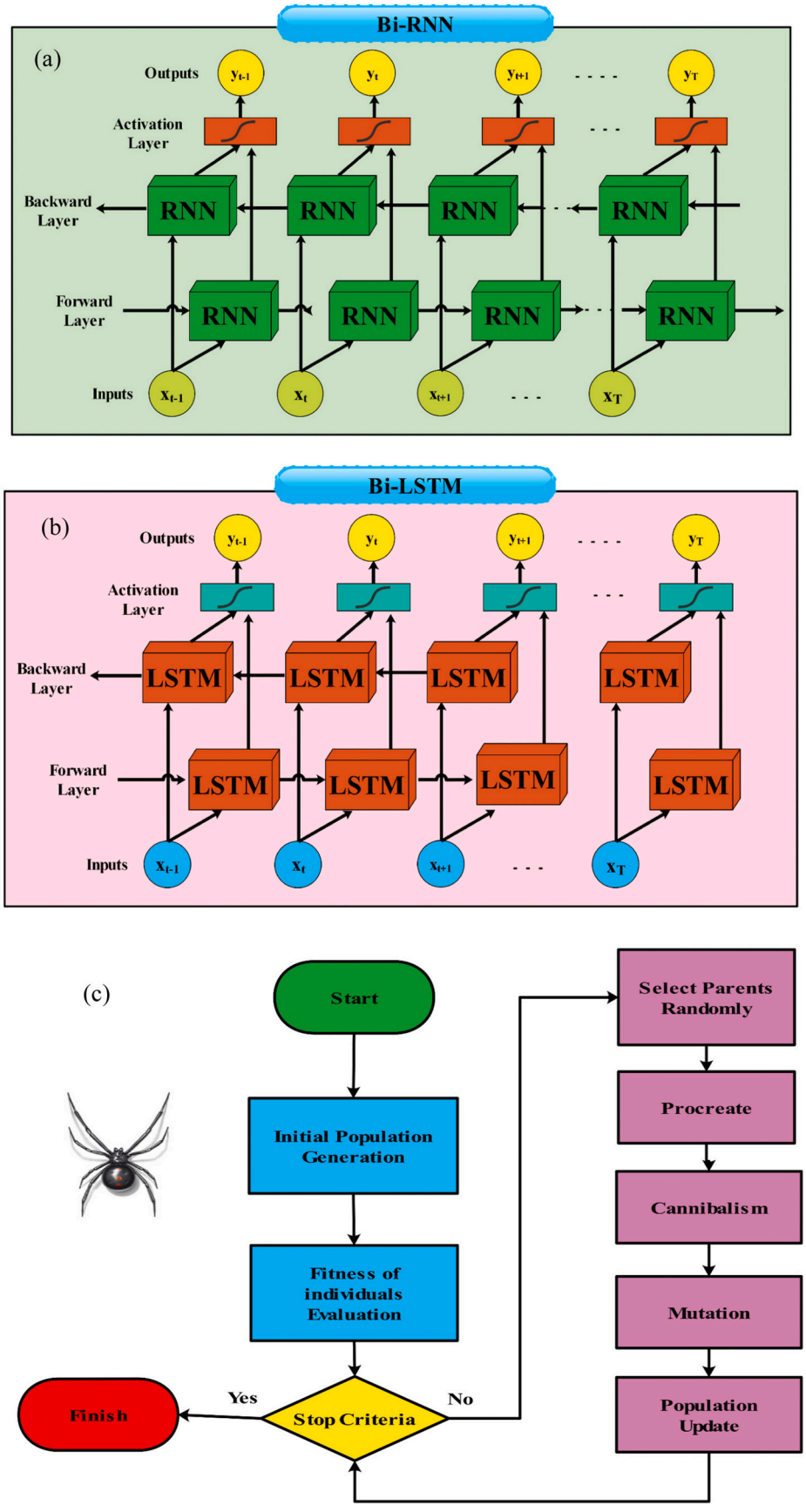

Fig. 5. Structure of the (a) BiRNN model (b) BiLSTM model and (c) BWO algorithm.

Table 2
Optimal Hyperparameter Values of the Models.

	Units	Dropout	Learning rate	Batch size	Epochs	Optimizer	Activation function
LSTM	38	0.2946	0.001	32	20	Adam	ReLU, Sigmoid
BiLSTM	14	0.1716	0.001	32	20	Adam	ReLU, Sigmoid
RNN	37	0.1386	0.001	32	20	Adam	ReLU, Sigmoid
BiRNN	36	0.3501	0.001	32	20	Adam	ReLU, Sigmoid
LSTM	20	0.3214	0.001	32	20	Adam	ReLU, Sigmoid
BiLSTM	17	0.2711	0.001	32	20	Adam	ReLU, Sigmoid
RNN	23	0.3209	0.001	32	20	Adam	ReLU, Sigmoid
BiRNN	23	0.2986	0.001	32	20	Adam	ReLU, Sigmoid

3.7.2. Feature selection using recursive feature elimination (RFE)

RFE systematically identifies the most critical features in a dataset by iteratively reducing the feature set. During the initial training phase, RFE trains the selected machine learning model (e.g., random forest), using all available features. It then ranks the features according to their significance or influence on the model's predictions or target variable (i.e. wildfires in the present study) (Guyon et al., 2002). The least important features are sequentially removed, and the model is re-trained with the remaining features. This cycle continues until the feature set is sufficiently reduced. The final model is then built using the optimal set of features that offer the highest predictive accuracy. The three main advantages of RFE are optimal feature identification, improved model interpretability, and increased efficiency.

3.8. Model performance

In the present study, a two-stage validation process was employed. Initially, the dataset was split into 80 % for training and 20 % for testing, with the test set rigorously excluded during all phases of model development to prevent data leakage (see Section 3.4. training and testing set for more details); the final model was evaluated solely on this holdout testing set to ensure an unbiased performance estimate (see Section 3.12. Model evaluation for more details). Subsequently, a 10-fold grid-based spatial cross-validation approach was applied exclusively to the training set using a specialized Python library (Sun et al., 2023) to assess spatial generalizability and mitigate potential bias from spatial autocorrelation. Traditional random cross-validation, which splits labeled data into training and validation sets, can overestimate model performance because spatially close points may share similar attributes, effectively allowing the model to "peek" into validation data. By partitioning data spatially rather than randomly, spatial cross-validation ensures greater independence between training and validation sets. More details about this approach provided by Abdollahi and Pradhan (2023).

3.9. Model theory and development

3.9.1. RNNs and BiRNNs

RNNs utilize an internal state to address sequential data (Schuster and Paliwal, 1997), thus it differs from deep neural networks in that it must incorporate information from previous inputs to affect the current inputs and outputs. Within each network layer, the RNN model implements weight parameters identical to those of the conventional deep neural networks (Dai et al., 2024).

Typically, an RNN generates hidden state h_i and outcome y_i at time step i. RNN structures that employ both of these are referred to as complete RNNs. h_i and y_i, which are interested in the planning of the unobserved states h_{i+1} with outcomes y_{i+1} at the subsequent time stage. The RNN employs h_i in the subsequent time step calculation. An Elman network is another term for this (Elman, 1990). The RNN requires only y_i, which is also referred to as an Elman network. In contrast, a Jordan RNN requires individual input (Cruse, 1996). The mathematical foundation of an RNN is as follows:

$$h_t = \sigma_h(W_h x_t + U_h h_{t-1} + b_h) \tag{3}$$

$$y_t = \sigma(W_y h_t + b_y) \tag{4}$$

where σ is the sigmoid function, and W_h, W_y, and U_h are weights that can be employed to generate the output, transmitted hidden state, and hidden states, respectively, from the previous time step. b_h and b_y are biases for the calculation of the hidden states and output, respectively.

BiRNN is an extended RNN containing layers that process sequential data in both forward and backward directions. BiRNN divides the standard unidirectional RNN state neurons to acquire both positive and negative sequential information (Schuster and Paliwal, 1997). Because they do not interact, any processed data, whether positive or negative, can be trained and updated in the same manner as a unidirectional RNN. The structure of the BiRNN model is presented in Fig. 5a.

3.9.2. LSTM and BiLSTM

Since conventional RNNs are prone to the vanishing gradient problem, we opted for an LSTM model in this study to overcome this limitation (Hochreiter and Schmidhuber, 1997). LSTM is a form of RNN that is capable of capturing long-term dependencies in sequential data, which is ideal for time-series analysis (Greff et al., 2016). The LSTM architecture consists of memory cells with three primary gates: input (i_{t_p}), forget (f_{t_p}), and output (o_{t_p}). These gates enable the network to write information into, read information from, and reset the cell state (Gers et al., 2000). The input gate determines what data is incorporated into the cell state, the forget gate decides which data is forgotten, and the output gate decides what data is passed onto the output. An LSTM layer has the following structure:

$$\mathrm{i}_{t_p} = \delta\left(\mathrm{W}_{xi}\mathrm{x}_{t_p} + \mathrm{W}_{Hi}\mathrm{H}_{t_{p-1}} + \mathrm{B}_i\right) \tag{5}$$

$$\mathrm{f}_{t_p} = \delta\left(\mathrm{W}_{xf}\mathrm{x}_{t_p} + \mathrm{W}_{Hf}\mathrm{H}_{t_{p-1}} + \mathrm{B}_f\right) \tag{6}$$

$$\mathrm{o}_{t_p} = \delta\left(\mathrm{W}_{x_0}\mathrm{x}_{t_p} + \mathrm{W}_{Ho}\mathrm{H}_{t_{p-1}} + \mathrm{B}_0\right) \tag{7}$$

$$\mathrm{c}_{t_p} = \mathrm{f}_{t_p} \odot \mathrm{c}_{t_{p-1}} + \mathrm{i}_{t_p} \odot tanh\left(\mathrm{W}_{xc}\mathrm{x}_{t_p} + \mathrm{W}_{Hc}\mathrm{H}_{t_{p-1}} + \mathrm{B}_c\right) \tag{8}$$

$$\mathrm{H}_{t_p} = \mathrm{o}_{t_p} \odot tanh\left(\mathrm{c}_{t_p}\right) \tag{9}$$

where $W(f, i, o, c)$ are the weights of the forget, input, output gates and cell state, respectively, while B_f, B_i, B_o, and B_c are the bias vectors for the forget, input, output gates and cell state, respectively. δ represents a sigmoid function. c_{t_p} is the memory cell state at t_p, x_{t_p} is the layer input, $\odot$is the element-wise product, tanh is the activation function for scaling values into the range of (−1,1), and $H_{t_{p-1}}$ is the final state or layer output at time $t-1$.

BiLSTM is an enhanced form of LSTM that takes into account the input sequence both forward and backward (Schuster and Paliwal, 1997). The BiLSTM architecture consists of two separate LSTM layers: one that processes the information in the input from left to right (forward) ($\overrightarrow{H}_{t_p}$) and one that processes it from right to left (backward) ($\overleftarrow{H}_{t_p}$). BiLSTM can model temporal dependencies in sequential data more

accurately than unidirectional LSTMs due to the fact that they incorporate both the past and future context. The output from both the forward and the backward LSTM layers can be concatenated or combined to produce the final output (u_{t_p}). Fig. 5b presents the structure of the BiLSTM model. In contrast to LSTM, which can only learn past and future dependencies in the forward direction, the BiLSTM layer can be concurrently trained as indicated by the following equation:

$$u_{t_p} = \psi\left(\overrightarrow{H}_{t_p}, \overleftarrow{H}_{t_p}\right) \tag{10}$$

3.9.3. Black widow optimization

The Black Widow Optimization (BWO) algorithm, a population-based metaheuristic inspired by the cannibalistic behavior of black widow spiders, was used to determine optimal hyperparameter values (Table 2). This algorithm can scan the search area and find a global optimal solution while avoiding local optimal solutions. It thus maintains a balance between exploration and exploitation via mutation (Hayyolalam and Pourhaji Kazem, 2020). BWO sets a potential answer as a "widow" in a manner similar to a "chromosome" and a "particle position" in GAs and particle swarm optimization (PSO), respectively. There is a possible answer called a "black widow spider" for some optimization problems that shows the values of the problem variables. The general phases of the BWO are as follows (Fig. 5c):

1. Initial population: the process begins by generating an initial population of spiders that represents potential solutions. Each solution is represented by a one-dimensional array.
2. Evaluation of individual fitness: Each widow's fitness is assessed in accordance with the problem-solving specifications using a fitness function.
3. Random selection of parents: if the halting criterion is not met, a set of mating spiders from the parents is chosen at random.
4. Reproduction: Each pair of spiders in the population generates a new generation. To prevent a generation of duplicated randomly selected widows, this phase continues for a number that is equal to half of the widows in the population (e.g., the number of partnerships).
5. Cannibalism: Three strategies (similar to neighborhood structures) are considered for the new generation, and one of them is implemented. These represent adolescent spiders and siblings who have reached sexual maturity. The fitness value is the determining factor for these. The sole organization that has access to this stage is the BWO. The new generation precludes solutions with an insufficient level of fitness in this scenario, which leads to early convergence.
6. Mutation: Mutation is performed by randomly swapping two elements within the array for each selected solution, allowing diversity to be maintained in the population.
7. Population Update: The population is refreshed with the newly generated individuals, and the best global solution is selected based on fitness evaluation.
8. Termination: A stopping criterion is established to determine whether the search should end with the current optimal solution or repeat steps 3 to 7 until the condition is met.

In Table 2, the number of units refers to the neurons in the hidden layers, while dropout represents the fraction of neurons dropped during training to prevent overfitting. The learning rate controls the step size during optimization, and the batch size specifies the number of samples processed before weight updates. Each model was trained for 20 epochs using the Adam optimizer. The Rectified Linear Unit (ReLU) activation function was applied in the hidden layers to introduce non-linearity, while the Sigmoid activation function was used in the output layer to generate probabilities for binary classification.

3.10. Wildfire susceptibility mapping

After developing and training, all eight standalone and hybrid deep learning models (i.e. LSTM, BiLSTM, RNN, BiRNN, LSTM-BWO, BiLSTM-BWO, RNN-BWO, and BiRNN-BWO) were used to generate the wildfire susceptibility map. In the first phase, the entire study area was transformed into a raster format with a pixel resolution of 4 km. Next, all eight trained models were used to predict the wildfire occurrence probability for each pixel of the study area. The wildfire occurrence probability values were then exported from Python into ArcGIS Pro (v3.4.0) and converted into wildfire susceptibility maps with five categories determined based on the quantile method: very low, low, moderate, high, and very high. This method is commonly employed for classification determination in datasets with skewed distributions (Akgun, 2012). Once the wildfire susceptibility map was generated, an analysis was conducted for each province in Canada to determine the percentage of the total land area that was susceptible to wildfire.

3.11. Interpretability

SHAP (SHapley Additive exPlanations) is a popular method for improving the interpretability of machine learning models by assigning each feature's contribution to the model's predictions. In the present study, SHAP value plot (beeswarm plots) were employed to address the black-box nature of the deep learning models used, providing interpretability and insights into their predictive behavior. SHAP values measure how much each feature positively or negatively influences a specific prediction (Pradhan et al., 2023).

3.12. Model evaluation

Several statistical measures and the receiver operating characteristic (ROC) were employed to quantitatively evaluate the performance of the models. The statistical measures considered in the present study were accuracy, precision, sensitivity, specificity, and the F1 score (Pham et al., 2016; Hong et al., 2023). Accuracy measured the percentage of both wildfire and non-wildfire pixels that were correctly classified, while precision represented the proportion of true wildfire samples correctly identified for all of the cases of predicted wildfires. Sensitivity measured the ratio of correctly identified wildfire cases to the total number of actual wildfires. Specificity indicated the ratio of correctly classified true non-wildfire cases to the total number of actual non-wildfire cases. The F1 score represents the harmonic average of a classification model's precision and recall. These metrics were calculated as follows:

$$\text{Accuracy} = ((TP + TN)/(TP + TN + FP + FN) \tag{11}$$

$$\text{Precision} = ((TP)/(TP + FP)) \tag{12}$$

$$\text{Recall/Sensitivity} = ((TP)/(TP + FN) \tag{13}$$

$$\text{Specificity} = ((TN)/(FP + TN)) \tag{14}$$

$$\text{F1 Score} = 2^{*}((\text{precision}^{*}\text{recall})/(\text{precision} + \text{recall})) \tag{15}$$

where TP, TN, FP, and FN are true positives (correctly classified as wildfires), true negatives (correctly classified as non-wildfires), false positives (incorrectly classified as wildfire), and false negatives (incorrectly classified as non-wildfires), respectively.

The ROC curve illustrates the performance of binary-based models. The curve plots sensitivity against the FP rate (FPR). The area under the ROC curve (AUC) serves as a quantitative indicator of model performance, with values ranging from 0.5 to 1. An AUC of 0.5 suggests a poor model, while an AUC of 1 represents an ideal model with optimal performance. The FPR is calculated as follows:

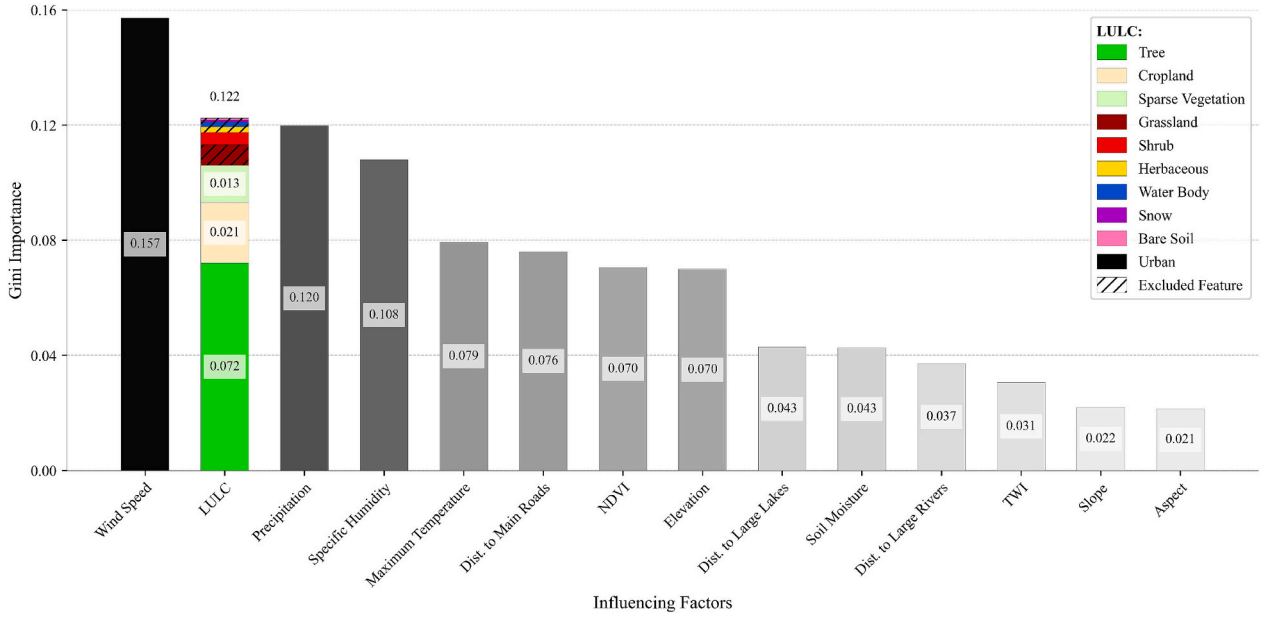

Fig. 6. Importance of geoenvironmental factors influencing the probability of wildfire occurrences based on the Gini Importance (GI) of a random forest model.

Table 3
Performance evaluation for the developed models (Bold values indicate the highest performance among unoptimized models, while shadow-bold values represent the highest overall performance).

	Standard deep-learning models				Optimized deep-learning models			
	LSTM	BiLSTM	RNN	BiRNN	LSTM-BWO	BiLSTM-BWO	RNN-BWO	BiRNN-BWO
Accuracy	**92.58**	92.19	86.75	90.60	95.35	**95.36**	94.59	95.12
Precision	90.70	**90.84**	85.63	89.46	93.41	**93.72**	93.49	93.21
Specificity	89.51	**89.90**	84.55	87.30	**93.07**	92.50	91.39	92.17
Sensitivity	**93.92**	93.58	88.64	92.58	96.74	**96.98**	96.40	96.88
F1 Score	**92.28**	92.19	87.11	90.99	95.04	**95.32**	94.92	95.01

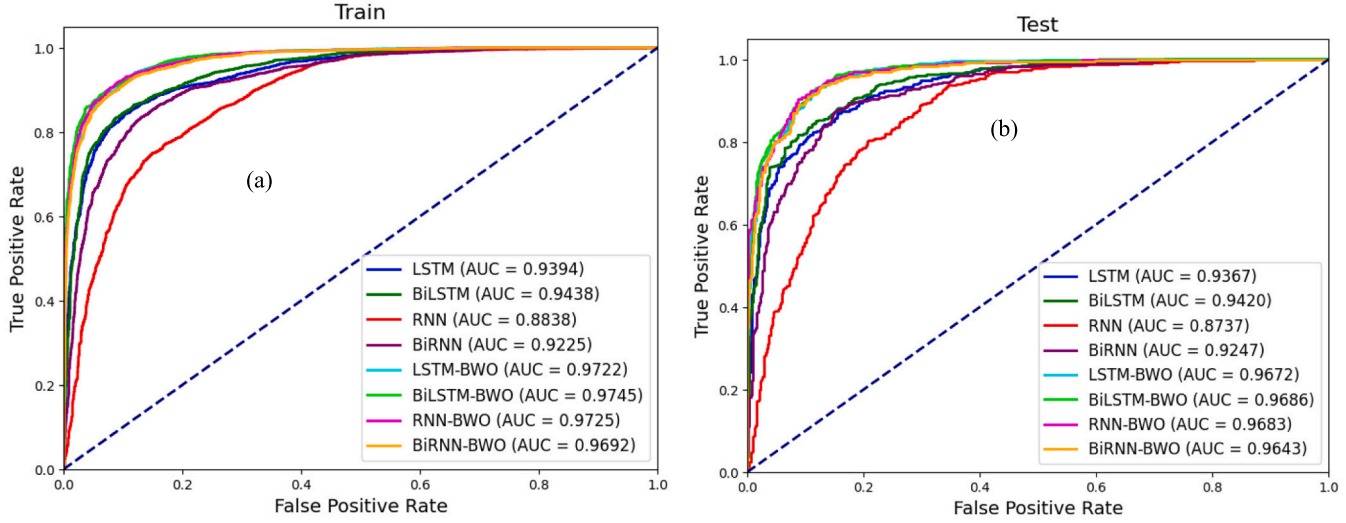

Fig. 7. Model performance evaluation based on ROC analysis during (a) training and (b) testing (the dotted black line shows the performance of a random guess).

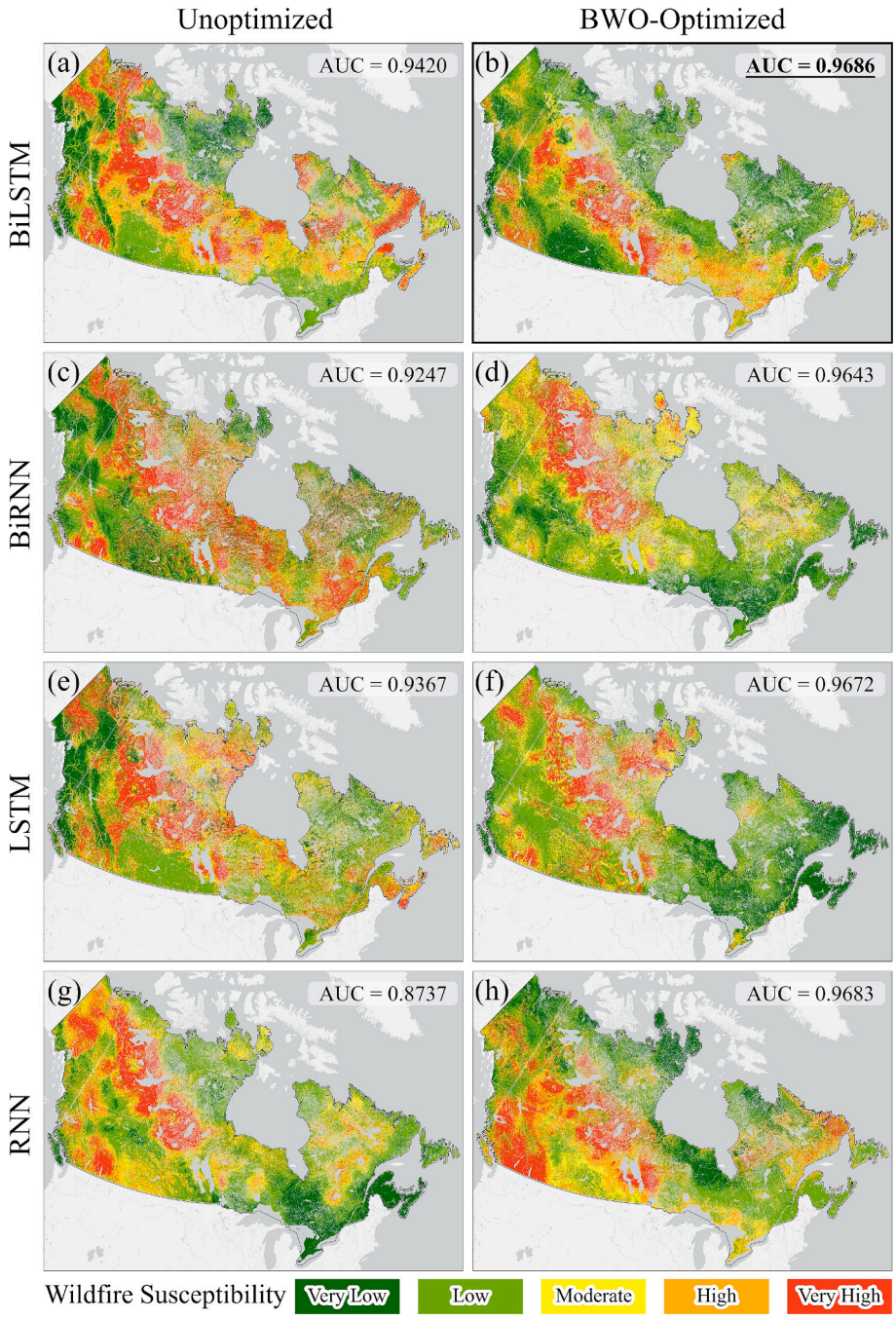

Fig. 8. Wildfire susceptibility maps derived from (a) BiLSTM, (b) BiLSTM-BWO, (c) BiRNN, (d) BiRNN-BWO, (e) LSTM, (f) LSTM-BWO, (g) RNN, and (h) RNN-BWO.

$$FPR = FP/(FP + TN) = 1\text{–specificity} \quad (16)$$

4. Results

4.1. Feature importance analysis

Assessing the importance of geoenvironmental variables provides valuable insights into their impact on wildfire occurrence. To optimize model performance, it is crucial to exclude factors that do not contribute to the predictive accuracy, thus reducing the model's complexity. In this study, the GI of the random forest algorithm was used to measure the influence of each input variable on the probability of wildfire occurrence. Wind speed (GI = 0.157) had the strongest impact on the wildfires, followed by LULC (0.122 cumulatively for all the LULC classes), precipitation (0.120), specific humidity (0.108), maximum temperature (0.079), distance from main roads (0.076), NDVI (0.070), elevation (0.077), distance from large lakes (0.043), soil moisture (0.043), distance from large rivers (0.037), TWI (0.031), slope (0.022) and aspect (0.021) (Fig. 6). Grasslands, water bodies, snow-covered areas, bare soil, and urban regions were excluded from the modeling process based on the results of RFE approach, leaving only cropland, tree-covered areas, and shrubland remanning among the predictors.

4.2. Model evaluation and analysis

The generated wildfire susceptibility maps were evaluated using various performance criteria (Table 3 and Fig. 7). The standalone LSTM model performed slightly better than BiLSTM model and outperformed

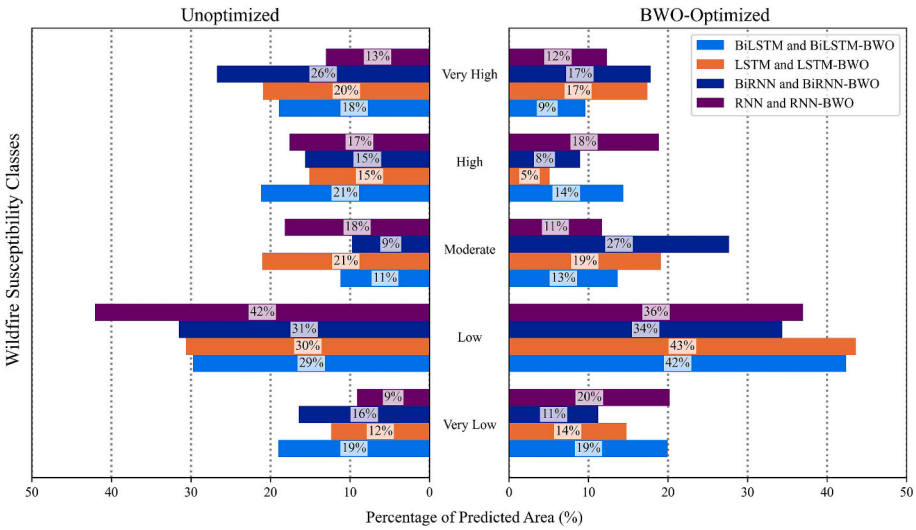

Fig. 9. Percentage area covered by each wildfire susceptibility class for each model.

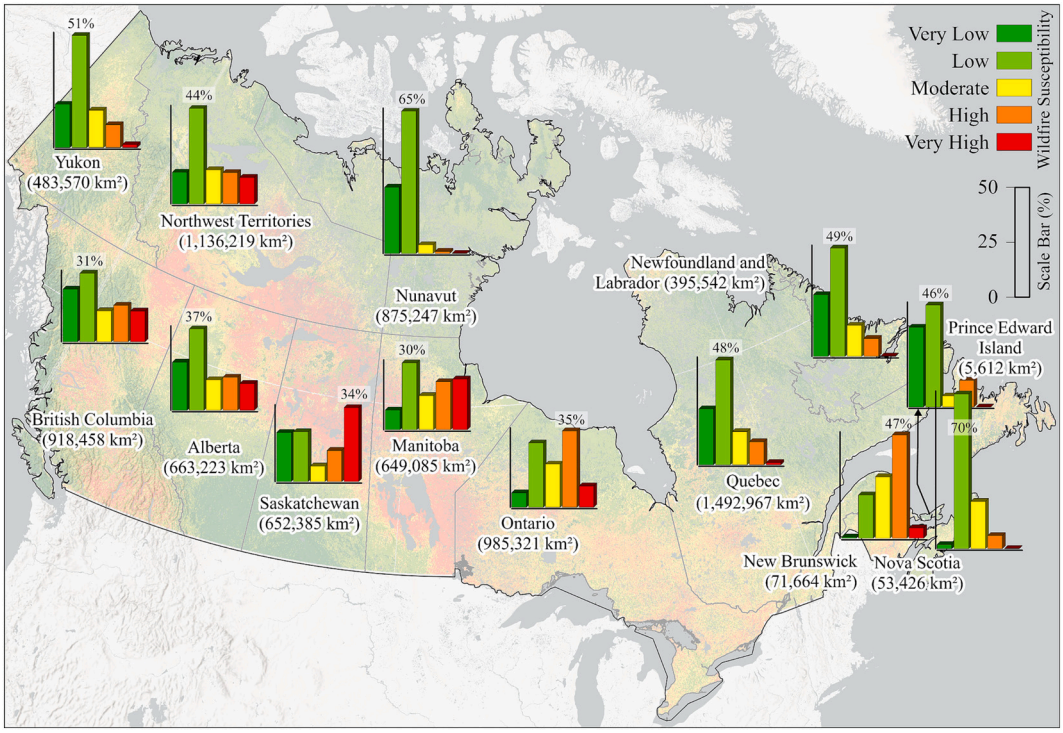

Fig. 10. Land area coverage of each wildfire susceptibility class by province/territory.

the other standalone models in terms of accuracy, sensitivity, and F1 score, while standalone BiLSTM model leads to the highest performance in precision and specificity. In terms of the optimized deep learning models, BiLSTM-BWO exhibited the highest performance for all metrics except of specificity. The results indicate that the optimized technique enhances the performance of BiLSTM more significantly than LSTM.

According to the classification by Yesilnacar and Topal (2005), all of the developed models exhibit an excellent performance in terms of the AUC, with values between 0.9 and 1.0, though the hybrid models outperformed the standalone models. In particular, during the training and testing phases, BiLSTM-BWO outperformed the other models with $AUC_{training} = 0.9745$ and $AUC_{testing} = 0.9686$, followed by RNN-BWO, LSTM-BWO, BiRNN-BWO, BiLSTM, BiRNN, LSTM and RNN in order.

BiLSTM-BWO improved on BiLSTM by about 2.82 % in terms of the AUC during testing, while BiLSTM improved on LSTM by 0.56 %. Overall, BiLSTM-BWO demonstrated a 3.40 % higher performance than the LSTM model.

4.3. *Wildfire susceptibility analysis*

This study employed both standard and optimized deep learning algorithms to create a wildfire susceptibility map on a national scale for Canada. The majority of Canada, particularly in the middle regions, exhibited a high to very high vulnerability to wildfires (Fig. 8). The unoptimized models tended to overestimate high/very high susceptibility areas compared to their optimized versions, especially in Ontario and Manitoba. According to BiLSTM-BWO, 19.7 %, 42.6 %, 13.4 %, 14.5 %, and 9.8 % of Canada had a very low, low, moderate, high, and

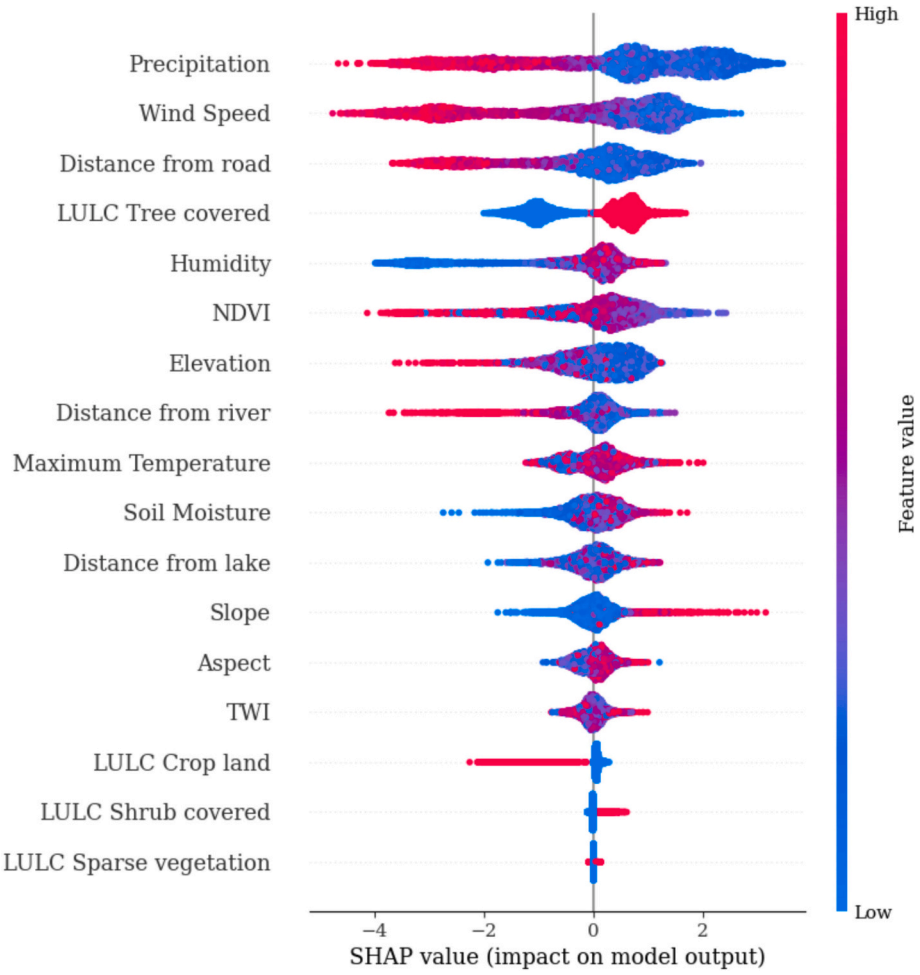

Fig. 11. Beeswarm plots illustrating the relationship between input variables and the output.

very high susceptibility to wildfire occurrences (Fig. 9).

The results by BiLSTM-BWO model revealed that 33.69 % of Saskatchewan—relative to the province's total area—had a very high susceptibility to wildfires, followed by Manitoba (23.10 %), British Columbia (14.03 %), and Alberta (12.19 %). By considering both high and very high classes, results shows that New Brunswick had the high and very high susceptibility (51.79 %), followed by Saskatchewan, Onterio, and British Columbina. In contrast, Prince Edward Island has the highest percentage of areas with a very low susceptibility to wildfires (93 %), followed by Newfoundland and Labrador (Fig. 10).

4.4. *Interpretability*

Fig. 11 showcases beeswarm plots depicting the distribution of low, high, and mean values for each feature within the training dataset (Matin and Pradhan, 2021). In other word, this image is used to interpret the contribution of predictive variables in a machine learning model. Specifically, the graph highlights the impact of geo-environmental and climatic variables on predicting the increasing or reducing of wildfires occurrences probability.

The plots reveal that variables such as precipitation, wind speed, distance from main roads, distance from large rivers and cropland LULC class have an inverse relationship with wildfire occurrence and consistently push the SHAP values toward the negative side, suggesting these features lower wildfire susceptibility. In contrast, tree covered LULC (given the prevalence of wildfires in vegetated areas), specific humidity, soil moisture, and slope have a direct relationship with features value and produce positive SHAP values, indicating an increased probability of wildfire when features value are high. NDVI, TWI and temperature do not show a distinct clustering toward positive or negative values, implying a relatively neutral net effect. Overall, precipitation, wind speed, distance from roads, and tree cover variables appear to significantly influence wildfire occurrence probability across Canada, as evidenced by SHAP values distributed widely along both the positive and negative ranges of the horizontal axis. By examining both the position (SHAP value) and color (feature magnitude) of each point, we gain insights into where threshold effects or interactions might be occurring—for example, high humidity (red points) is moderately associated with elevated wildfire, whereas dry conditions (low humidity) predominantly reduce the predicted probability of wildfire. The distinct separation of LULC feature points into red and blue, divided by positive and negative SHAP values, arises from the binary encoding of each constituent LULC class. Red points for these features indicate the presence (binary value of 1) of that specific class, while blue points indicate its absence (binary value of 1). Overall, these findings highlight the most influential factors driving the model's predictions and provide a transparent, instance-level interpretation of how individual predictors shape wildfire occurrence estimates across Canada.

5. Discussion

Wildfires represent a serious threat in Canada, with the area affected by fires steadily increasing in recent decades. This has had detrimental effects on natural resources and increased the risk to communities and infrastructure at the boundary between natural and urban/residential areas. Therefore, it is important to map wildfire-prone areas in Canada

in order to mitigate wildfire risks and reduce the associated costs through proactive prevention and risk management. In this context, deep learning models offer a robust approach to identifying wildfire-susceptible regions by considering multiple factors based on historical wildfire records. In this study, four standalone deep learning models (LSTM, BiLSTM, RNN, and BiRNN) and their counterparts optimized with the BWO algorithm were used to produce a total of eight wildfire susceptibility maps for all of Canada.

5.1. Input geoenvironmental variables

In the present study, wind speed, LULC, precipitation, specific humidity, maximum temperature, distance from main roads and NDVI were found to be the most important indicators of wildfire probability across Canada as a whole, which was in accordance with the current understanding of wildfire occurrences. For example, the NDVI and LULC are indicative of the material available to be burnt. Jaafari et al. (2019) reported that most wildfires in the Golestan province of Iran occur in areas with an NDVI higher than 0.5. In addition, Prasad et al. (2008) found that the primary factor influencing wildfire occurrences was the mean annual temperature, while Rezaie et al. (2023) revealed that the majority of wildfires in Hawaii occurred at temperatures higher than 23 °C, while no wildfires were reported for areas with temperatures lower than 19 °C. Higher temperatures can lead to a higher evaporation rate and reduced moisture levels in vegetation, raising the likelihood of a fire outbreak (Guo et al., 2016).

As in the present study, Rezaie et al. (2023) reported that most wildfires occurred close to roads. Tran et al. (2023) also showed that the distance from roads is the strongest indicator of wildfire occurrence on Oahu Island, US, followed by temperature. The same results have also been reported by Catry et al. (2009) and Liu et al. (2015b). The proximity to roads is closely associated with human activities, which are the primary cause of wildfires in Canada. Roadways can act as ignition points, whether from vehicle emissions, improperly discarded cigarette waste, or by offering access to areas more vulnerable to wildfires, such as locations with dry vegetation or accumulated dead trees. In another study, Abdollahi and Pradhan (2023) implemented SHAP plots and deep learning models for wildfires in Australia. They revealed that factors such as rainfall, humidity, elevation, wind speed, slope, and the normalized difference moisture index (NDMI) played critical roles in influencing the model's output for wildfire susceptibility mapping. In summary, previous research emphasizes that the significance of geoenvironmental factors varies by region, indicating that data collection must be tailored to the unique attributes of each study area.

As reported by the government of British Columbia, the majority of wildfires in the province are sparked by lightning strikes. In contrast, in Alberta, human actions are the primary factor behind wildfire outbreaks. These activities include off-road vehicles, campfires, fireworks, ammunition, industrial work, agriculture, and power lines. Gaur et al. (2021) also revealed that global warming in Canada is likely to lead to a longer wildfire season and more extreme wildfire events around Canadian cities, with Nelson in British Columbia and Thunder Bay in Ontario particularly at risk. These findings thus emphasize the need to adapt city infrastructure to the higher wildfire threat.

5.2. Model selection and reliability

Canada has about 367 million hectares of forest (3,670,000 km^2) and, due to their importance, these areas need to be protected. Because Canada has a large land area and a high number of historical wildfires, deep learning models are well-suited for wildfire susceptibility predictions in this country. The higher flexibility, end-to-end learning, and ability to handle complex data are other advantages of these models. Deep learning models consistently improve as more data becomes available, making them well-suited for large-scale applications. Their multiple layers enable the modeling of highly complex, non-linear relationships that are often beyond the capabilities of shallow models (Ertuğrul et al., 2024). The deep learning algorithms used in the present study effectively captured the intricate and nonlinear connections between wildfire data and the 14 geoenvironmental influencing factors without requiring predefined assumptions about the functional form needed to describe the underlying physics.

Our results revealed that, although the standalone deep learning models were accurate and flexible, optimization increased their prediction power. Tuning the hyperparameters of deep learning models can be challenging, thus the BWO algorithm was employed in the present study. BWO performs well in both the exploitation and exploration phases, offering rapid convergence and effectively avoiding local optima. Additionally, it maintains a well-balanced approach between exploration and exploitation (Hayyolalam and Pourhaji Kazem, 2020).

It was found that BiLSTM was superior to the other models. BiLSTM harnesses the strengths of LSTM in terms of handling long-term dependencies while also incorporating future context by integrating both forward and backward LSTM layers (Kulshrestha et al., 2020). LSTM, a specialized form of RNN, was originally developed to address the challenges associated with capturing long-term dependencies in sequential data. It achieves this by incorporating memory cells and gating mechanisms to manage the flow of information. In addition, unlike the LSTM and RNN models, BiLSTM processes the sequence in both directions (i.e. forward or backward) at the same time.

5.3. Comparison with past studies

Rezaie et al. (2023) implemented GMDH and CNN models combined with biogeography-based optimization (BBO) and ant colony optimization (ACO) to generate a wildfire susceptibility map for Maui, US. In total, 1745 historical wildfire locations were recorded and used for modeling. They revealed that the CNN outperformed GMDH, with ACO (AUC = 0.885) slightly enhancing the results compared to BBO. However, all of the models tested in the present study were more accurate than those produced by Rezaie et al. (2023), even their CNN model.

Jaafari et al. (2019) hybridized ANFIS with a GA, PSO, a shuffled frog leaping algorithm (SFLA), and an imperialist competitive algorithm (ICA) for wildfire mapping in Golestan province, Iran. They reported that ANFIS-ICA (AUC = 0.99) outperformed the other models, while the ANFIS (0.90) had the weakest performance. The slightly higher performance of ANFIS-ICA compared to the models in the present study may originate from their smaller study area. In larger areas, the pixel size may need to be increased, leading to lower performance. It should be noted that our standalone models still had a much higher prediction power than the ANFIS model (0.90). Hong et al. (2019) integrated the Weights-of-Evidence (WOE) bivariate model with the Analytical Hierarchy Process (AHP) model for forest fire prediction in Huichang County, China, achieving an AUC between 0.91 and 0.94. This performance is lower than the predicted results of our study, which is conducted at a national scale. Zhang et al. (2019) implemented a CNN algorithm for wildfire susceptibility mapping in Yunnan Province, China, reporting reasonable results with an accuracy of 0.86.

Bjånes et al. (2021) prepared wildfire susceptibility maps for Biobío and Ñuble, Chile, using CNN, SVM, and extreme gradient boosting models. They found that the CNN model, with an AUC of 0.902, outperformed the other machine learning models. Tran et al. (2023) also combined GMDH with BBO, ICA, and TLBO for the wildfire mapping of Oahu Island, US. They reported that GMDH-TLBO, with an AUC of 0.81, was the best-performing model. However, our developed models, even our standalone models, exhibited a higher performance than their hybrid algorithms.

5.4. Limitations and uncertainty

In the present study, a 80:20 ratio was implemented for data splitting and the development of the training and testing datasets. While there are

no strict guidelines for dividing training and testing datasets, an 80:20 ratio is widely adopted in machine learning. Nevertheless, this ratio can still lead to some uncertainty. Another potential source of uncertainty in the present study was the selection of non-wildfire locations, even though Euclidean distance to the nearest historical wildfire location approach has been considered in random generation of those points. In addition, in the present study, only large wildfire data was considered for modeling. It should be noted that considering all number of wildfires could ensure that the results are more robust.

Due to the large size of Canada, most of the data used in the present study was collected using remotely sensed sources. The resolution of the digital elevation model and other input variables was satisfactory given the size of the study area, but the resolution has an impact on modeling accuracy (Qiu et al., 2022). Therefore, the proposed models may still not be as accurate as the ground-truth data. Furthermore, historical wildfire data collection focused exclusively on large occurrences, excluding smaller fires from the dataset. This reliance on historical data may not fully capture future wildfire patterns, and there may be other influencing factors that were not considered in the present study. Future research could thus explore the inclusion of additional factors with a larger historical wildfire dataset.

5.5. Challenges and outlook for practical applications

The developed hybrid deep learning models, particularly the BiLSTM-BWO model, hold significant potential for real-world applications in wildfire management, including fire warning systems, resource allocation, and policy-making. By integrating the models with real-time data streams, they can support dynamic updates for early warning systems, prioritize resource deployment in high-risk areas, and guide post-disaster recovery efforts. However, practical implementation faces challenges such as ensuring the timeliness and quality of data acquisition, addressing computational demands, and adapting the models to regional variations. Solutions like automated data pipelines, cloud-based computing, and GIS-based platforms can enhance usability, while collaboration among researchers, policymakers, and emergency responders will be crucial for effective deployment and maximizing the models' impact.

6. Conclusion

This study successfully applied four standalone (LSTM, BiLSTM, RNN, and BiRNN) and optimized (LSTM-BWO, BiLSTM-BWO, RNN-BWO, and BiRNN-BWO) deep learning models for wildfire susceptibility mapping across Canada. A dataset containing 4240 historical wildfires recorded between 2014 and 2023, as well as 14 geoenvironmental factors, was collected. A random forest Gini index and RFE were then implemented to determine the optimal input parameters. All of the developed models and their wildfire-susceptibility maps were evaluated using statistical measures and the AUC-ROC method.

It was found that the wind speed had the strongest impact on wildfire occurrences, followed by LULC (cumulatively including all LULC classes), total precipitation, specific humidity, maximum temperature, distance from main roads, NDVI, elevation, distance from large lakes, soil moisture, distance from large rivers, TWI, slope, and aspect. Based on the outcomes of the GI and RFE methods, grasslands, water bodies, snow-covered zones, bare soil, and urban areas of LULC classes were excluded as predictors from the modeling process, leaving only croplands, tree-covered regions, and shrublands as LULC predictors for the analysis. Areas covered by trees demonstrate a direct and strong association with wildfire across Canada.

While all of the models performed well, the hybrid models outperformed their standalone counterparts. The overall ranking of the models in terms of performance was BiLSTM-BWO > RNN-BWO > LSTM-BWO > BiRNN-BWO > BiLSTM > LSTM > BiRNN > RNN. The BiLSTM-BWO model classified 19.7 %, 42.6 %, 13.4 %, 14.5 %, and 9.8 % of Canada as having very low, low, moderate, high, and very high susceptibility to wildfires, respectively. Saskatchewan is the most vulnerable provinces to future wildfire occurrences followed by Manitoba, British Columbia, and Alberta. Conversely, Prince Edward Island had the highest proportion of very low wildfire susceptibility areas followed by Newfoundland and Labrador.

The findings from the present study offer actionable insights for wildfire risk mitigation strategies in Canada. The proposed models demonstrated reasonable accuracy, and the resulting susceptibility maps can be employed in wildfire risk assessment and strategic management. Decision-makers and governmental bodies can use these precision-driven maps to implement targeted interventions, optimize resource allocation, and enhance preparedness efforts, thereby significantly reducing the potential impact of wildfires in vulnerable regions.

Acknowledgment and funding

The authors would like to thank the Natural Sciences and Engineering Council of Canada (NSERC Discovery Grant), the Department of Environment, Energy and Climate Action, the Government of Prince Edward Island, and the Atlantic Canada Opportunities Agency for their financial support of this research study. Special thanks to the Canadian Centre for Climate Change and Adaptation, University of Prince Edward Island for providing this opportunity to work on this research project. This collaborative work was also supported by Korea Environment Industry & Technology Institute through Innovative Flood Protection Technologies against Climate Crisis Program, funded by Korea Ministry of Environment (RS-2023-00218873, 50 % contribution), as well as the National Research Foundation of Korea grants funded by the Korea Government (RS-2023-00222333 & RS-2021-NR060085).

CRediT authorship contribution statement

Khabat Khosravi: Software, Methodology, Formal analysis, Data curation, Conceptualization, Writing – review & editing, Writing – original draft. **Ashkan Mosallanejad:** Software, Methodology, Formal analysis, Data curation, Conceptualization. **Sayed M. Bateni:** Methodology, Conceptualization, Writing – review & editing. **Dongkyun Kim:** Methodology, Conceptualization, Writing – review & editing. **Changhyun Jun:** Methodology, Conceptualization, Writing – review & editing. **Ali Reza Shahvaran:** Software, Methodology, Formal analysis, Data curation. **Aitazaz A. Farooque:** Validation, Supervision, Methodology, Conceptualization, Writing – review & editing. **Massoud Karbasi:** Conceptualization, Writing – original draft. **Mumtaz Ali:** Conceptualization, Writing – original draft.

Consent to participate

Not applicable.

Consent for publication

Not applicable.

Ethics approval

Not applicable.

Author statement

During the preparation of this work, the authors used ChatGPT just to correct spelling and grammar. After using this tool/service, the authors reviewed and edited the content as needed and take full responsibility for the content of the publication.

Declaration of competing interest

The authors declare that there is no conflict of interest associated with this research or manuscript.

Data availability

Data will be provided under reasonable request from the corresponding author. Geospatial layers used as model inputs were obtained from the following sources:

Elevation data were obtained from the USGS EarthExplorer data hub (http://earthexplorer.usgs.gov;last accessed 1 January 2025). Slope, aspect, and topographic wetness index (TWI) layers were derived from the elevation using built-in tools in ArcGIS Pro (v3.4.0). Soil moisture, precipitation, wind speed, and maximum temperature data are publicly available from TerraClimate through Goggle Earth Engine (https://developers.google.com/earth-engine/datasets/catalog/IDAHO_EPSCOR_TERRACLIMATE;last accessed 1 January 2025), whereas specific humidity data were downloaded from NASA FLDAS data catalog (https://developers.google.com/earth-engine/datasets/catalog/NASA_FLDAS_NOAH01_C_GL_M_V001;last accessed 1 January 2025). LULC data were retrieved from the FAO Land Resources Planning Toolbox (https://www.fao.org/land-water/land/land-governance/land-resources-planning-toolbox/category/details/en/c/1036355/;last accessed 1 January 2025), and NDVI data originated from AVHRR and VIIRS satellite imagery through open government datahub (https://open.canada.ca/data/en/dataset/44ced2fa-afcc-47bd-b46e-8596a25e446e;last accessed 1 January 2025). Finally, distances from roads and major waterbodies (rivers and lakes) were calculated using the Government of Canada's Road Network dataset (https://www12.statcan.gc.ca/census-recensement/2011/geo/rnf-frr/index-eng.cfm;last accessed 1 January 2025) and the National Hydro Network (https://open.canada.ca/data/en/dataset/a4b190fe-e090-4e6d-881e-b87956c07977; last accessed 1 January 2025), respectively. Historical large wildfire data points can also be accesses through Government of Canada's LFDB database (https://cwfis.cfs.nrcan.gc.ca/datamart/metadata/lfdb;last accessed 1 January 2025).

References

Abatzoglou, J.T., Brown, T.J., 2012. A comparison of statistical downscaling methods suited for wildfire applications. Int. J. Climatol. 32, 772–780. https://doi.org/10.1002/joc.2312.

Abatzoglou, J.T., Dobrowski, S.Z., Parks, S.A., Hegewisch, K.C., 2018. TerraClimate, a high-resolution global dataset of monthly climate and climatic water balance from 1958–2015. Sci. Data 5, 170191. https://doi.org/10.1038/sdata.2017.191.

Abdollahi and Pradhan, 2023. Explainable artificial intelligence (XAI) for interpreting the contributing factors feed into the wildfire susceptibility prediction model. Sci. Total Environ. 879, 163004.

Achu, A.L., Thomas, J., Aju, C.D., Gopinath, G., Kumar, S., Reghunath, R., 2021. Machine-learning modelling of fire susceptibility in a forest-agriculture mosaic landscape of southern India. Eco. Inform. 64, 101348. https://doi.org/10.1016/j.ecoinf.2021.101348.

Akgun, A., 2012. A comparison of landslide susceptibility maps produced by logistic regression, multi-criteria decision, and likelihood ratio methods: A case study at İzmir. Turkey. Landslides 9 (1), 93–106. https://doi.org/10.1007/s10346-011-0283-7.

Alizadeh, M.R., Abatzoglou, J.T., Adamowski, J., et al., 2023. Elevation-dependent intensification of fire danger in the western United States. Nat. Commun. 14, 1773. https://doi.org/10.1038/s4 1467-023-37311-4.

Angayarkkani, K., Radhakrishnan, N., 2011. An effective technique to detect forest fire region through ANFIS with spatial data. 2011 3rd International Conference on Electronics Computer Technology. IEEE.

Arrue, B.C., Ollero, A., De Dios, J.M., 2000. An intelligent system for false alarm reduction in infrared forest-fire detection. IEEE Intel. Syst. Applic. 15 (3), 64–73.

Barmpoutis, P., Dimitropoulos, K., Kaza, K., Grammalidis, N., 2019. Fire detection from images using faster R-CNN and multidimensional texture analysis. ICASSP 2019-2019 IEEE International Conference on Acoustics. Speech and Signal Processing (ICASSP), IEEE.

Bjånes, A., De La Fuente, R., Mena, P., 2021. A deep learning ensemble model for wildfire susceptibility mapping. Eco. Inform. 65, 101397. https://doi.org/10.1016/j.ecoinf.2021.101397.

Breiman, L., Friedman, J., Olshen, R. and Stone, C. (1984) Classification and Regression Trees. Chapman and Hall, Wadsworth, New York, PP 368. eBook ISBN9781315139470.

Carmo, M., Moreira, F., Casimiro, P., Vaz, P., 2011. Land use and topography influences on wildfire occurrence in northern Portugal. Landsc. Urban Plan. 100, 169–176 [Google Scholar] [CrossRef] [Green Version].

Catry, F.X., Rego, F.C., Baçao, F.L., Moreira, F., 2009. Modeling and mapping wildfire ignition risk in Portugal. Int. J. Wildland Fire 18, 921–931. https://doi.org/10.1071/WF07123.

Chen, G., Guo, Y., Yue, X., Tong, S., Gasparrini, A., Bell, M.L., Armstrong, B., Schwartz, J., Jaakkola, J.J., Zanobetti, A., 2021. Mortality risk attributable to wildfire-related PM2· 5 pollution: a global time series study in 749 locations. Lancet Planet. Health 5 (9), e579–e587.

Chen, H., Zhang, W., Sheng, L., 2025a. Canadian record breaking wildfire in 2023 and their impact on US air quality. Atmos. Environ. 342, 120941. https://www.sciencedirect.com/science/article/abs/pii/S1352231024006162.

Chen, H., Zhang, W., Sheng, L., 2025b. Canadian record-breaking wildfires in 2023 and their impact on US air quality. Atmos. Environ. 342, 120941.

Cordoba, A., Vilar, R., Lavrov, A., Utkin, A., Fernandes, A., 2004. Multi-objective optimisation of lidar parameters for forest-fire detection on the basis of a genetic algorithm. Opt. Laser Technol. 36 (5), 393–400.

Cruse, H., 1996. Neural networks as cybernetic systems. Thieme Stuttgart.

Dai, Y., Wei, J., Qin, F., 2024. Recurrent neural network (RNN) and long short-term memory neural network (LSTM) based data-driven methods for identifying cohesive zone law parameters of nickel-modified carbon nanotube reinforced sintered nano-silver adhesives. Mater. Today Commun. 39, 108991.

Di Giuseppe, F., Rémy, S., Pappenberger, F., Wetterhall, F., 2018. Using the Fire Weather Index (FWI) to improve the estimation of fire emissions from fire radiative power (FRP) observations. Atmos. Chem. Phys. 18 (8), 5359–5370.

Doerr, S.H., Santín, C., 2016. Global trends in wildfire and its impacts: perceptions versus realities in a changing world. Philos. Trans. R. Soc. B Biol. Sci. 371 (1696), 20150345.

Elman, J.L., 1990. Finding structure in time. Cogn. Sci. 14, 179–211.

Ertuğrul, O.F., Guerrero, J.M., Yilmaz, M., 2024. Shallow Learning vs. A Practical Guide for Machine Learning Solutions. Softcover, Deep Learning. ISBN978-3-031-69501-8Due: 27 October 2025. DOIdoi:10.1007/978-3-031-69499-8.

Gaur, A., Enichou, N., Armstrong, M., Hill, F., 2021. Potential future changes in wildfire weather and behavior around 11 Canadian cities. Urban Clim. 35 (2021), 100735.

Gers, F.A., Schmidhuber, J., Cummins, F., 2000. Learning to forget: Continual prediction with LSTM. Neural Comput. 12, 2451–2471.

Greff, K., Srivastava, R.K., Koutník, J., Steunebrink, B.R., Schmidhuber, J., 2016. LSTM: A search space odyssey. IEEE Trans. neural networks Learn. Syst. 28, 2222–2232.

Guo, F., Zhang, L., Jin, S., Tigabu, M., Su, Z., Wang, W., 2016. Modeling anthropogenic fire occurrence in the boreal forest of China using logistic regression and random forests. Forests 7, 1–14. https://doi.org/10.3390/f7110250.

Guyon, I., Weston, J., Barnhill, S., Vapnik, V., 2002. Gene selection for cancer classification using support vector machines. Mach. Learn. 46 (2002), 389–422.

Hanes, C.C., et al., 2019. Fire-regime changes in Canada over the last half century. Can. J. Res. 49, 256–269.

Hayyolalam, V., Pourhaji Kazem, A., 2020. Black Widow Optimization Algorithm: A novel meta-heuristic approach for solving engineering optimization problems. Eng. Appl. Artif. Intell. 87, 103249.

Hochreiter, S., Schmidhuber, J., 1997. Long short-term memory. Neural Comput. 9, 1735–1780.

Hong, H., Tsangaratos, P., Ilia, I., Liu, J., Zhu, A., Xu, C., 2018. Applying genetic algorithms to set the optimal combination of forest fire related variables and model forest fire susceptibility based on data mining models. The case of Dayu County. China Haoyuan. Sci. Total Environ. 630 (2018), 1044–1056. https://doi.org/10.1016/j.scitotenv. 2018.02.278.

Hong, H., Jaafari, A., Zenner, E., 2019. Predicting spatial patterns of wildfire susceptibility in the Huichang County, China: An integrated model to analysis of landscape indicators. Ecol. Indic. 101, 878–891. https://doi.org/10.1016/j.ecolind.2019.01.056.

Hong, X., Liu, C., Zhang, C., Tian, Y., Wu, H., Yin, H., Zhu, Y., Cheng, Y., 2023. Vast ecosystem disturbance in a warming climate may jeopardize our climate goal of reducing CO2: a case study for megafires in the Australian 'black summer'. Sci. Total Environ. 866, 161387.

Horn, K.H., Vulova, S., Li, H., Kleinschmit, B., 2025. Modelling current and future forest fire susceptibility in north-eastern Germany. Nat. Hazards Earth Syst. Sci. 25, 383–401. https://doi.org/10.5194/nhess-25-383-2025.

Iban, M.C., Sekertekin, A., 2022. Machine learning based wildfire susceptibility mapping using remotely sensed fire data and GIS: a case study of Adana and Mersin provinces. Turkey. Ecol. Inform. 69, 101647. https://doi.org/10.1016/j.ecoinf.2022.101647.

Jaafari, A., Zenner, E., Panahi, M., Shahabi, H., 2019. Hybrid artificial intelligence models based on a neuro-fuzzy system and metaheuristic optimization algorithms for spatial prediction of wildfire probability. Agric. For. Meteorol. 266–267 (2019), 198–207.

Jain, P., Coogan, S.C., Subramanian, S.G., Crowley, M., Taylor, S., Flannigan, M.D., 2020. A review of machine learning applications in wildfire science and management. Environ. Rev. 28 (4), 478–505.

Jakubowski, J., Solarczyk, M., Wiśnios, M., 2019. Smoke detection in a digital image with the use of convolutional network. SPIE, XII Conference on Reconnaissance and Electronic Warfare Systems.

Janizadeh, S., Batenni, S.M., Jun, C., Im, J., Pai, H.T., Band, S., Mosavi, A., 2023. Combination four different ensemble algorithms with the generalized linear model (GLM) for predicting forest fire susceptibility. Geomat. Nat. Haz. Risk 14 (1), 2206512.

Janizadeh, S., Tran, T.H., Bateni, S.M., Jun, C., Kim, D., Trauernicht, C., Heggy, E., 2024. Advancing the LightGBM approach with three novel nature-inspired optimizers for predicting wildfire susceptibility in Kaua'i and Moloka'i Islands. Hawaii. Expert Systems with Applications 258, 124963. https://doi.org/10.1016/j.eswa.2024.124963.

Khennou, F., Akhloufi, M.A., 2023. Improving wildland fire spread prediction using deep U-Nets. Sci. Remote Sens. 8, 100101. https://www.sciencedirect.com/science/article/pii/S2666017223000263.

Ko, B., Cheong, K.-H., Nam, J.-Y., 2010. Early fire detection algorithm based on irregular patterns of flames and hierarchical Bayesian Networks. Fire Saf. J. 45 (4), 262–270.

Kulshrestha, Krishnaswamy, A.V., Sharma, M., 2020. Bayesian BILSTM approach for tourism demand forecasting. Ann. Tour. Res. 83 (2020), 102925.

Latham, J., Cumani, R., Rosati, I., Bloise, M., 2014. Global land cover share (GLC-SHARE) database beta-release version 1.0-2014. FAO 29.

Li, T., Zhao, E., Zhang, J., Hu, C., 2019. Detection of wildfire smoke images based on a densely dilated convolutional network. Electronics 8 (10), 1131.

Li, X., Song, W., Lian, L., Wei, X., 2015. Forest fire smoke detection using back-propagation neural network based on MODIS data. Remote Sens. 7 (4), 4473–4498.

Li, X., Chen, Z., Wu, Q.J., Liu, C., 2018. 3D parallel fully convolutional networks for real-time video wildfire smoke detection. IEEE Trans. Circuits Syst. Video Technol. 30 (1), 89–103.

Liu, Y., Yang, Y., Liu, C., Gu, Y., 2015a. Forest fire detection using artificial neural network algorithm implemented in wireless sensor networks. ZTE Commun. 13 (2), 12–16.

Liu, Z., Wimberly, M.C., Lamsal, A., Sohl, T.L., Hawbaker, T.J., 2015b. Climate change and wildfire risk in an expanding wildland – urban interface: a case study from the Colorado Front Range Corridor. Landsc. Ecol. 30, 1943–1957. https://doi.org/10.1007/S10980-015-0222-4.

Mahony, C.R., Wang, T., Hamann, A., Cannon, A.J., 2022. A global climate model ensemble for downscaled monthly climate normals over North America. Int. J. Climatol. 42, 5871–5891. https://doi.org/10.1002/joc.7566.

Masoudian, E., Mirzaei, A., Bagheri, H., 2025. Assessing wildfire susceptibility in Iran: Leveraging machine learning for geospatial analysis of climatic and anthropogenic factors. Trees, Forests and People 19, 100774.

Masrur, A., Yu, M., Taylor, A., 2023. Capturing and interpreting wildfire spread dynamics: attention-based spatiotemporal models using ConvLSTM networks. Eco. Inform. 82, 102760.

Massada, A. Bar, Syphard, A.D., Hawbaker, T.J., Stewart, S.I., Radeloff, V.C., 2011. Effects of ignition location models on the burn patterns of simulated wildfires. Environ. Model. Softw. 26, 583–592. https://doi.org/10.1016/j.envsoft.2010.11.016.

Matin, S., Pradhan, B., 2021. Earthquake-Induced Building-Damage Mapping Using Explainable AI (XAI). Sensors 21 (2021), 4489.

McNally, A., 2018. FLDAS Noah Land Surface Model L4 Global Monthly 0.1 x 0.1 degree (MERRA-2 and CHIRPS). Goddard Earth Sciences Data and Information Services Center (GES DISC), Greenbelt, MD, USA. Accessed: 10.5067/5NHC22T9375G.

Mell, W., Jenkins, M.A., Gould, J., Cheney, P., 2007. A physics-based approach to modelling grassland fires. Int. J. Wildland Fire 16 (1). https://doi.org/10.1071/WF06002.

Moreira, F., Rego, F.C., Ferreira, P.G., 2001. Temporal (1958–1995) pattern of change in a cultural landscape of northwestern Portugal: Implications for fire occurrence. Landsc. Ecol. 16, 557–567.

Moreira, F., Vaz, P., Catry, F., Silva, J.S., 2009. Regional variations in wildfire susceptibility of land-cover types in Portugal: implications for landscape management to minimize fire hazard. Int. J. Wildland Fire 18, 563–574.

Muhammad, K., Ahmad, J., Baik, S.W., 2018. Early fire detection using convolutional neural networks during surveillance for effective disaster management. Neurocomputing 288, 30–42.

Pal, M., 2005. Random forest classifier for remote sensing classification. Int. J. Remote Sens. 26 (1), 217–222.

Panahi, M., Khosravi, K., Rezaie, F., Ferreira, C.S.S., Destouni, G., Kalantari, Z., 2023. A country wide evaluation of Sweden's spatial flood modeling with optimized convolu- tional neural network algorithms. Earth's. Future 11. https://doi.org/10.1029/2023EF003749 e2023EF003749.

Pham, B.T., Pradhan, B., Bui, D.T., Prakhsh, I., Ramayanti, M.B., 2016. A comparative study of different machine learning methods for landslide susceptibility assessment: A case study of Uttarakhand area (India). Environ. Model Softw. 84, 240–250.

Pradhan, B., Lee, S., Dikshit, A., Kim, H., 2023. Spatial flood susceptibility mapping using an explainable artificial intelligence (XAI) model. Geosci. Front. 14 (6), 101625.

Prasad, K.S.N., Ramakrishna, S., 2008. An autonomous forest fire detection system based on spatial data mining and fuzzy logic. Int. J. Comp. Sci. Network Secur. 8 (12), 49–55.

Prasad, V.K., Badarinath, K.V.S., Eaturu, A., 2008. Biophysical and anthropogenic controls of forest fires in the Deccan Plateau. India. J. Environ. Manag. 86, 1–13. https://doi.org/10.1016/J.JENVMAN.2006.11.017.

Qiu, L., Chen, J., Fan, L., Sun, L., Zheng, C., 2022. High-resolution mapping of wildfire drivers in California based on machine learning. Sci. Total Environ. 833, 155155.

Ramayanti, S., Kim, B., Park, S., Lee, C., 2024. Wildfire susceptibility mapping by incorporating damage proxy maps, differenced normalized burn Ratio, and deep learning algorithms based on sentinel-1/2 data: a case study on Maui Island. Hawaii. GISci. Remote Sens. 61 (1), 2353982.

Regina International Airport, 2015. Canadian Climate Normals 1981–2010. Environment Canada. September 25, 2013. Archived from the original on May 18.

Rezaie, F., Panahi, M., Bateni, S.M., Lee, S., Jun, C., Trauernicht, C., Neale, C., 2023. Development of novel optimized deep learning algorithms for wildfire modeling: A case study of Maui, Hawai'i. Eng. Appl. Artif. Intell. 125 (2023), 106699.

Roy, T., Shome, S.K., 2023. Optimization of RNN-LSTM Model Using NSGA-II Algorithm for IOT-based Fire Detection Framework. IETE J. Res. 70 (7), 6239–6254. https://www.tandfonline.com/doi/full/10.1080/03772063.2023.2287637.

Saha, S., Bera, B., Shit, P.K., Trauernicht, S., Sengupta, N., 2023. Prediction of forest fire susceptibility applying machine and deep learning algorithms for conservation priorities of forest resources. Remote Sensing Applications: Soc. Environ. 29, 100917. https://doi.org/10.1016/j.rsase.2022.100917.

Sayad, Y.O., Mousannif, H., Al Moatassime, H., 2019. Predictive modeling of wildfires: A new dataset and machine learning approach. Fire Saf. J. 104, 130–146.

Schuster, M., Paliwal, K.K., 1997. Bidirectional recurrent neural networks. IEEE Trans. Signal Process. 45, 2673–2681. https://doi.org/10.1109/78.650093.

Smellie, Sarah, June 12, 2023. Nearly 350 firefighters from the EU will help battle relentless Canadian wildfires. CTV News. Archived from the original on June 16, 2023. Retrieved June 16, https://www.ctvnews.ca/canada/article/nearly-350-firefighters-from-the-eu-will-help-battle-relentless-canadian-wildfires/.

Sturtevant, B.R., Scheller, R.M., Miranda, B.R., Shinneman, D., Syphard, A., 2009. Simulating dynamic and mixed-severity fire regimes: a process-based fire extension for LANDIS-II. Ecol. Model. 220 (23), 3380–3393. LANDIS-II. Ecol. Model. 220, 3380–3393. https://doi.org/10.1016/j.ecolmodel.2009.07.030.

Sun, K., Hu, Y., Lakhanpal, G., Zhou, R.Z., 2023. Spatial cross-validation for GeoAI. In: Gao, S., Hu, Y., Li, W. (Eds.), Handbook of Geospatial Artificial Intelligence. Taylor & Francis Group. https://www.taylorfrancis.com/books/edit/10.1201/9781003308423.

Tang, R., Mao, J., Jin, M., Chen, A., Yu, Y., Shi, X., Zhang, Y., Hoffman, F.M., Xu, M., Wang, Y., 2021. Interannual variability and climatic sensitivity of global wildfire activity. Adv. Clim. Chang. Res. 12 (5), 686–695.

Tehrany, M.S., Pradhan, B., Jebur, M.N.M.N., 2014. Flood susceptibility mapping using a novel ensemble weights-of-evidence and support vector machine models in GIS. J. Hydrol. 512, 332–343. https://doi.org/10.1016/j.jhydrol.2014.03.008.

The State of Canada's Forests Report, 2023. Government of Canada. June 11, 2015. Archived from the original on July 19. Retrieved August 1, 2023.

Tran, T., Bateni, S., Rezaie, F., Panahi, M., Jun, C., Trauernicht, C., Neale, C., 2023. Enhancing predictive ability of optimized group method of data handling (GMDH) method for wildfire susceptibility mapping. Agric. For. Meteorol. 339 (2023), 109587.

Le, H. Van, Hoang, D.A., Tran, C.T., Nguyen, P.Q., Tran, V.H.T., Hoang, N.D., Amiri, M., Ngo, T.P.T., Nhu, H.V., Hoang, T. Van, Tien Bui, D., 2021. A new approach of deep neural computing for spatial prediction of wildfire danger at tropical climate areas. Eco. Inform. 63, 101300. https://doi.org/10.1016/j.ecoinf.2021.101300.

Wang, T., Hamann, A., Spittlehouse, D., Carroll, C., 2016. Locally Downscaled and Spatially Customizable Climate Data for Historical and Future Periods for North America. PLoS One 11, e0156720. https://doi.org/10.1371/journal.pone.0156720.

Wang, Y., Yu, C., Tu, R., Zhang, Y., 2011. Fire detection model in Tibet based on grey-fuzzy neural network algorithm. Expert Syst. Appl. 38 (8), 9580–9586.

Wang, Y., Dang, L., Ren, J., 2019. Forest fire image recognition based on convolutional neural network. J. Algorithms Computat. Technol. 13, 174830261 9887689.

Wang, Z., Wang, Z., Zou, Z., Chen, X., Wu, H., Wang, W., Su, H., Li, F., Xu, W., Liu, Z., 2024. Severe global environmental issues caused by Canada's record-breaking wildfires in 2023. Springer.

Xue, H., Gu, F., Hu, X., 2012. Data assimilation using sequential Monte Carlo methods in wildfire spread simulation. ACM Trans. Model. Comput. Simul. 22. https://doi.org/10.1145/2379810.2379816.

Yesilnacar, E., Topal, T., 2005. Landslide susceptibility mapping: a comparison of logistic regression and neural networks methods in a medium scale study, Hendek Region (Turkey). Eng. Geol. 79 (3–4), 251–266. https://doi.org/10.1016/j.enggeo.2005.02.002.

Yuan, J., Wang, L., Wu, P., Gao, C., Sun, L., 2018. Detection of wildfires along transmission lines using deep time and space features. Pattern Recognition and Image Analysis 28, 805–812.

Zhang, B., Wei, W., He, B., Guo, C., 2018. Early wildfire smoke detection based on improved codebook model and convolutional neural networks. Tenth International Conference on Digital Image Processing (ICDIP 2018), SPIE.

Zhang, G., Wang, M., Liu, K., 2019. Forest Fire Susceptibility Modeling Using a Convolutional Neural Network for Yunnan Province of China. Int. J. Disaster Risk Sci. 10, 386–403. https://doi.org/10.1007/s13753-019-00233-1.

Zhang, Q., Xu, J., Xu, L., Guo, H., 2016. Deep convolutional neural networks for forest fire detection. 2016 International forum on management. Atlantis Press, Education and information technology application.

Zhao, J., Zhang, Z., Han, S., Qu, C., Yuan, Z., Zhang, D., 2011. SVM based forest fire detection using static and dynamic features. Comput. Sci. Inf. Syst. 8 (3), 821–841.